

Ranking and Tuning Pre-trained Models: A New Paradigm of Exploiting Model Hubs

Kaichao You¹ *

YOUKAICHAO@GMAIL.COM

Yong Liu¹ *

LIUYONG21@MAILS.Tsinghua.EDU.CN

Ziyang Zhang²

ZHANGZIYANG11@HUAWEI.COM

Jianmin Wang¹

JIMWANG@TSINGHUA.EDU.CN

Michael I. Jordan³

JORDAN@CS.BERKELEY.EDU

Mingsheng Long¹ †

MINGSHENG@TSINGHUA.EDU.CN

¹ *School of Software, BNRist, Tsinghua University, Beijing 100084, China.*

² *Advanced Computing and Storage Lab, Huawei Technologies Co. Ltd*

³ *Division of Computer Science and Department of Statistics, UC Berkeley, CA 94720-1776, USA*

Editor: Stefan Harmeling

Abstract

Model hubs with many pre-trained models (PTMs) have been a cornerstone in deep learning. Although built at a high cost, they remain *under-exploited*: practitioners usually pick one PTM from the provided model hub by popularity and then fine-tune the PTM to solve the target task. This naïve but common practice poses two obstacles to sufficient exploitation of pre-trained model hubs: (1) the PTM selection by popularity has no optimality guarantee; (2) only one PTM is used while the rest PTMs are ignored. Ideally, to exploit pre-trained model hubs maximally, trying all combinations of PTMs and extensively fine-tuning each PTM combination are required, which incurs exponential combinations and an unaffordable computational budget. In this paper, we propose a new paradigm of exploiting model hubs by ranking and tuning pre-trained models: (1) Our conference paper (You et al., 2021) proposed LogME to estimate the maximum value of label evidence given features extracted by pre-trained models, which can rank all the PTMs in a model hub for various types of PTMs and tasks *before fine-tuning*. (2) The best ranked PTM can be fine-tuned and deployed if we have no preference for the model’s architecture, or the target PTM can be tuned by top-K ranked PTMs via the proposed B-Tuning algorithm. The ranking part is based on the conference paper, and we complete its theoretical analyses in this paper, including the convergence proof of the heuristic evidence maximization procedure and the influence of feature dimension. The tuning part introduces a novel Bayesian Tuning (B-Tuning) method for tuning multiple PTMs, which surpasses specialized methods designed for tuning homogeneous PTMs and sets up a new state of the art for tuning heterogeneous PTMs. The new paradigm of exploiting PTM hubs can be interesting to a large audience across the machine learning community.

Keywords: Pre-trained Model Hub, Model Ranking, Model Tuning, Transfer Learning

*. The first two authors contribute equally to the paper.

†. Mingsheng Long is the corresponding author.

1. Introduction

Deep neural networks (He et al., 2015, 2016; Devlin et al., 2019) trained by large-scale data (Deng et al., 2009; Russakovsky et al., 2015; Merity et al., 2017) and specialized computational devices (Jouppi et al., 2017) has achieved better performance than human on many recognition tasks in both computer vision and natural language processing. Lots of researchers (Donahue et al., 2014; Girshick et al., 2014; Devlin et al., 2019) found that deep neural networks trained on a large-scale pre-training task (Yang et al., 2019; Clark et al., 2020; Brown et al., 2020) can produce generic representations (Donahue et al., 2014) that benefit downstream tasks such as object detection (Girshick et al., 2014) and language understanding (Wang et al., 2019). These trained neural networks are known as pre-trained models (PTMs). Readers can refer to dedicated surveys (Han et al., 2021; Qiu et al., 2020; Bommasani et al., 2021) for a holistic overview of pre-trained models. The amazing power (Brown et al., 2020) of PTMs, together with the transfer learning paradigm of “pre-training → fine-tuning” to exploit PTMs, has revolutionized both vision (Kornblith et al., 2019) and language (Devlin et al., 2019) communities, and PTMs’ influence is spreading to more communities like geometric learning (Hu et al., 2020).

The cost of training PTMs varies from hundreds of GPU *hours* (He et al., 2016) to hundreds of GPU *days* (Devlin et al., 2019), which is too expensive for individual researchers and academic labs to afford. Most pre-trained models are provided by technical tycoons, including PyTorch Hub¹, TensorFlow Hub², and HuggingFace Transformer Models³. A collection of pre-trained models is called a “pre-trained model hub” (PTM Hub), which has become an indispensable ingredient in practitioners’ daily development. Take the HuggingFace Transformer library (Wolf et al., 2020) for example, the most popular BERT model (Devlin et al., 2019) is downloaded over 80 million times every month!

Although technical tycoons spent enormous resources on providing rich PTM Hubs for the public, it turns out that practitioners usually *pick the most popular PTM*, meaning that the whole PTM Hub is insufficiently exploited. Figure 1 analyzes the monthly downloads of PTMs in the HuggingFace Transformer hub. Except for several popular models, the rest PTMs in the hub are seldom downloaded. The statistics in PyTorch Hub and TensorFlow Hub are quite the same: several popular PTMs dominate the rest.

Naïvely picking the most popular PTM is far from optimal in two aspects: (1) The PTM selection is *task-specific* and one PTM cannot be optimal for all the tasks: different tasks favor different PTMs, depending on the compatibility between the pre-trained model and the target task (You et al., 2021). (2) Only one PTM is exploited, and the rest PTMs are put aside. Correspondingly, there are two reasons why practitioners resort to the suboptimal naïve practice: (1) maximally exploiting a PTM hub requires trying all combinations of PTMs and extensively fine-tuning each PTM combination, which requires unaffordable exponential computation; (2) even if the humongous computational cost can be paid, it is unclear how to exploit multiple PTMs in transfer learning. As pointed out in Section 2.4, Shu et al. (2021) studied the problem in a limited case, but a general solution is still missing.

1. <https://pytorch.org/hub/>

2. <https://www.tensorflow.org/hub>

3. <https://huggingface.co/models>

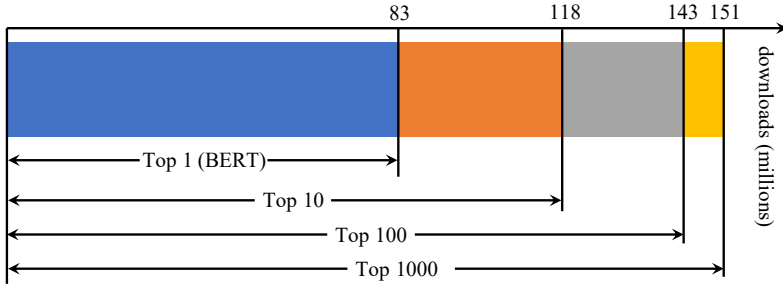


Figure 1: Monthly download statistics (in millions) for top popular models in the Hugging-Face Transformer library. The most popular PTM (BERT) takes up more than a half downloads, while other PTMs are much less exploited.

To fully exploit PTM hubs, we propose a new paradigm: ranking and tuning pre-trained models. Figure 2 provides an overview of the paradigm. It consists of two parts: (1) PTMs are *ranked* by a transferability metric; (2) top-ranked PTMs are *tuned* to meet downstream applications’ requirements. Our preliminary work (You et al., 2021) proposed LogME to estimate the compatibility between PTMs and downstream datasets, and demonstrated its effectiveness on a variety of PTMs and tasks, well supporting the ranking of PTMs. With a provided transferability rank, the best ranked PTM can be fine-tuned if there are no constraints on network architecture like inference time or hardware-friendly operators. If these constraints are present, the qualified PTM with desired architecture might not be the best-ranked one, but it can be tuned by top-K ranked PTMs via a novel B-Tuning algorithm proposed in Section 5.3.

Compared with picking the most popular PTM, our proposed new paradigm features two significant advantages: (1) it provides a *task-adaptive ranking* of all PTMs in a PTM hub to enable optimal selection of PTMs; (2) it opens the new possibility to *exploit multiple PTMs for tuning*, breaking the stereotype that fine-tuning must be tied up with a single PTM. The new paradigm can be useful in a broad variety of scenarios, as pre-trained models are increasingly important in deep learning.

Besides a new paradigm of exploiting PTM hubs, this paper brings novel theoretical analyses and a new algorithm for multiple PTMs tuning. (1) On the theoretical side, we derive the sufficient condition for the evidence maximization algorithm (MacKay, 1992) to converge and analyze the influence of dimensionality on LogME. The evidence maximization algorithm (MacKay, 1992) has been supposed to be purely heuristic for decades, and to the best of our knowledge, we are the first to successfully derive its convergence condition. (2) On the algorithm design side, we devise B-Tuning for tuning multiple PTMs using Bayesian learning, which surpasses the dedicated method (Shu et al., 2021) for homogeneous PTMs (PTMs with the same architecture) and also works for the challenging scenario with heterogeneous PTMs (PTMs with different architectures).

The contributions of this paper are summarized as follows:

1. We propose a new paradigm of exploiting PTM hubs, namely ranking and tuning pre-trained models. It has significant advantages compared with the common practice of naively fine-tuning a popular pre-trained model.

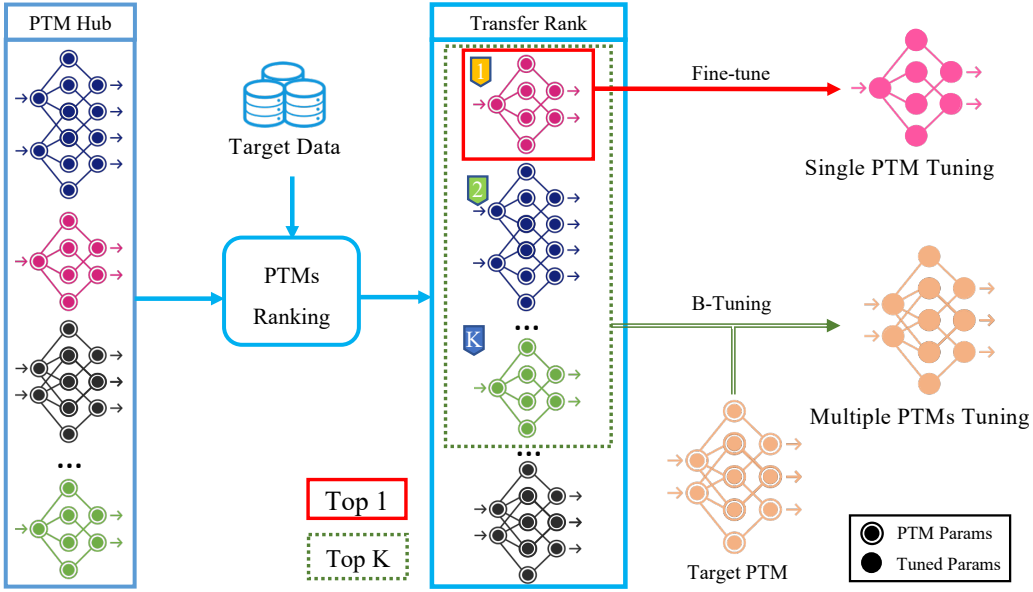


Figure 2: The proposed paradigm of ranking and tuning pre-trained models. PTMs are ranked by their transferability w.r.t. the target data, then either the best PTM is fine-tuned, or the target PTM is tuned by top- K PTMs via the proposed B-Tuning.

2. Concerning ranking PTMs, we propose LogME for transferability assessment and develop a fast algorithm to accelerate the computation. LogME is easy to interpret and is extremely efficient: it brings at most $3700\times$ speedup in wall-clock time and requires just 1% memory footprint compared with brute-force fine-tuning. Theoretical analyses confirm the rationality of LogME, and lay a theoretical foundation for a decades-long heuristic algorithm in evidence maximization.
3. For tuning PTMs, two possible scenarios are studied. In the academic scenario without specific requirements for the PTM architecture, the best ranked pre-trained model according to the transferability rank can be selected for subsequent fine-tuning; in the industrial scenario where a specific PTM architecture is required to meet the budget of computation and energy, we propose B-Tuning to tune the given pre-trained model with top- K ranked PTMs, even though these PTMs are heterogeneous.

Compared with our conference paper (You et al., 2021) that only proposed LogME for transferability estimation, this paper extends LogME to a paradigm of ranking and tuning pre-trained models. Additional theoretical analyses are available in the ranking part, and a new algorithm is presented in the tuning part. Moreover, LogME is tested against additional tasks like named entity recognition (Sang and De Meulder, 2003) in Section 6.2.5 and prompt learning (Liu et al., 2021a) in Section 6.6.

Note that this paper contains heavy math and many notations. For the convenience of readers, all the notations and their meanings are listed in Table 9 for reference. The basic problem setup contains a PTM hub with M pre-trained models $\{\phi_k\}_{k=1}^M$, and the transfer learning task is given by a labeled dataset $\mathcal{D} = \{(x_i, Y_i)\}_{i=1}^n$ with n labeled data

points. This paper focuses on classification and regression tasks, so the label $Y_i \in \mathbb{R}^C$ is C dimensional. Before this paper, it is common practice to select a popular pre-trained model ϕ and to fine-tune it on the target task. To sufficiently exploit the PTM hub, we propose a new paradigm of “ranking and tuning pre-trained models”.

The rest of the paper is organized as follows: Section 2 summarizes related work, Section 3 focuses on ranking and introduces a transferability metric named LogME, Section 4 holds theoretical analyses about LogME, Section 5 focuses on tuning and introduces a novel B-Tuning method for multiple PTMs tuning, Section 6 holds all the experiments, and finally Section 7 concludes the paper.

2. Related work

2.1 Transfer learning

Transfer learning (Thrun and Pratt, 1998) consists of transductive transfer, inductive transfer, task transfer, and so on. A well-known transductive paradigm is domain adaptation (Quionero-Candela et al., 2009), which aims for reducing domain shifts by transferring samples, hidden features (Long et al., 2015; Ganin and Lempitsky, 2015), and categorical information (Cao et al., 2022). Inductive transfer, namely fine-tuning in deep learning (Erhan et al., 2010; Yosinski et al., 2014), exploits prior knowledge (pre-trained models) to improve the performance of target tasks. Task transfer learning (Zamir et al., 2018) focuses on how to transfer tasks rather than pre-trained models. It aims to discover the relevance among tasks (Ben-David and Schuller, 2003) and to exploit the relationship for improvement on the target task. In the context of deep learning, transfer learning usually means inductive transfer with a pre-trained model, which is the focus of this paper.

Many previous works (Yosinski et al., 2014; Kornblith et al., 2019; Neyshabur et al., 2020) revealed the benefit of initializing a deep neural network with a pre-trained model. Apart from the vanilla method (*i.e.*, the pre-trained model is just used for initialization), researchers have recently proposed sophisticated fine-tuning techniques like regularization (Li et al., 2018; Chen et al., 2019), additional supervision (You et al., 2020), and carefully designed architecture (Kou et al., 2020). They can further improve transfer learning performance, but empirically *these fine-tuning methods do not change the ranking of pre-trained models on downstream tasks*. That is, if pre-trained model A is better than pre-trained model B after vanilla fine-tuning, empirically A is better than B when those advanced techniques are integrated. For example, on three datasets and four sampling rates in Table 2 of You et al. (2020), better fine-tuning performance primarily indicates better Co-Tuning (their proposed method) performance, implying that the transferability of a pre-trained model might be *task-specific* rather than *method-specific*. Therefore, our experiments stick to the vanilla fine-tuning during PTM ranking.

2.2 PTMs and PTM hubs

Pre-trained models (PTMs) are generalizable deep networks trained on large-scale data. They can be transferred to a series of downstream tasks. They have become a cornerstone in deep learning and sometimes are known as foundation models (Bommasani et al., 2021). Typical categories of PTMs are summarized in the following.

Supervised PTMs. In the ImageNet classification challenge, He et al. (2015) developed the first deep neural network that surpassed human performance. By supervised pre-training on the ImageNet dataset, deep models marched towards higher accuracy, fewer parameters, and lower computation. InceptionNet (Szegedy et al., 2015) made use of parallel convolutional filters to extract different levels of features. ResNet (He et al., 2016) introduced skip-connections to ease the vanishing gradient problem so that much deeper networks could be trained. Inspired by ResNet, DenseNet (Huang et al., 2017) was equipped with dense skip-connections to reuse features in a parameter-efficient manner. MobileNet (Sandler et al., 2018) was a low-parameter, mobile-friendly network structure which was further optimized with the help of network architecture search to become MNASNet (Tan et al., 2019).

Unsupervised PTMs. Although supervised pre-training is the most common practice, the labeling cost of large-scale data is too expensive to afford. As a large amount of unlabeled data on the Internet are available but under-exploited, recently many researchers have sought to apply self-supervised learning (Jing and Tian, 2020) on unlabeled data (Mahajan et al., 2018) with contrastive loss (Gutmann and Hyvärinen, 2010). And then, a family of unsupervised deep models has emerged in recent years. He et al. (2020) proposed Momentum Contrast with a creative queue structure to fully exploit the manifold structure of unlabeled data. Chen et al. (2020a) greatly improved the performance by exploring data augmentation, multi-layer projection head, and empirical designs. Designing better strategies for contrastive pre-training is still under active research (Tian et al., 2020).

Language PTMs. In recent years, natural language processing, the crown jewel of artificial intelligence, has been revolutionized by language PTMs. Unsupervised pre-trained models have been well established by training masked language models (Devlin et al., 2019) or autoregressive language models (Yang et al., 2019) on large unlabeled corpora (Merity et al., 2017). Liu et al. (2019) explored many practical details on how to improve the training of language models. Sanh et al. (2019) proposed distillation to make PTMs smaller and faster. These pre-trained language models are very common in winning submissions on important benchmarks like GLUE (Wang et al., 2018) and SQuAD (Rajpurkar et al., 2016), and have established their profound influence in the industry.

PTMs are grouped together to be hosted in PTM Hubs like TorchVision and HuggingFace Models. Technical giants spent humongous resources on training so many PTMs, but unfortunately, PTM Hubs are rather under-exploited, as quantitatively measured in Figure 1 and described in the introduction section in detail. The goal of this paper is to develop a new paradigm of exploiting PTM hubs, so that pre-trained models can be sufficiently exploited.

2.3 Assessing the transferability of pre-trained models

Assessing the transferability of PTMs has great significance in guiding the practice of deep learning. It can be used to rank available PTMs and act as a criterion for pre-trained model selection. Yosinski et al. (2014) studied the performance of transferring different layers of a pre-trained model, and Kornblith et al. (2019) studied a wide variety of ImageNet PTMs with modern network architectures. These papers aim for a deep understanding (Neyshabur et al., 2020) of transfer learning by expensive and exhaustive fine-tuning with humongous computation cost (see Section 6.5), which is hard for practitioners to afford. In most scenarios, practitioners care most about PTMs’ relative ranking on target tasks to guide

PTM selection, requiring a practical assessment method that is *efficient*, *accurate*, and *general*: a transferability assessment method should be efficient enough compared with brute-force fine-tuning (Zamir et al., 2018), should be accurate enough to identify potentially best models, and should be general enough to tackle a wide variety of common scenarios.

LEEP (Nguyen et al., 2020) and NCE (Tran et al., 2019) were the first two methods to assess the transferability of pre-trained models. Nguyen et al. (2020) constructed an empirical predictor from the joint distribution $p(y_t, y_s)$ over pre-trained labels y_s and target labels y_t , and calculated the log expectation of the empirical predictor (LEEP) as the transferability measure. The empirical predictor predicts the probability of the target class y_t as $\sum_{y_s \in \mathcal{Y}_s} p(y_t|y_s)p(y_s)$, where $p(y_s)$ comes from the PTM’s prediction over pre-trained categories. Negative Conditional Entropy (NCE) proposed by Tran et al. (2019) depended on an information-theoretic quantity (Cover, 1999) to reveal the transferability and hardness between different tasks. It estimated the joint distribution $p(y_t, y_s)$ with one-hot labels and predictions, and defined NCE as $-H(y_t|y_s)$, *i.e.*, the negative conditional entropy of target labels y_t given PTM’s predictions y_s .

Table 1: Applicability of existing methods and LogME proposed in this paper.

Modality	Pre-train	Target	Method		
			LEEP	NCE	LogME
vision	classification	classification	✓	✓	✓
	classification	regression	✗	✗	✓
	contrastive	classification	✗	✗	✓
	contrastive	regression	✗	✗	✓
language	language modeling	classification	✗	✗	✓

However, the above methods left plenty of room for further improvement. As shown in Table 1, they can only handle classification tasks with supervised pre-trained models. Increasingly popular contrastive pre-trained models and language models are out of their scope. The LogME algorithm proposed in this paper greatly extends the applicability of transferability assessment. LogME is fast to compute, less prone to over-fitting, and broadly applicable to various pre-trained models/downstream tasks/data modalities. Its performance is validated by extensive experiments. Prior to this paper, for most (4 out of 5) transfer learning settings, task adaptive transferability assessment did not have a decent solution. In addition, LogME’s statistical rigor makes it extensible to multiple PTMs tuning (see Section 5.3), which completes the new paradigm of ranking and tuning pre-trained models.

2.4 Multiple PTMs tuning

The straightforward approach in transfer learning is to fine-tune models initialized from pre-trained parameters, which we call “*single PTM tuning*” because it can only exploit a specific pre-trained model during fine-tuning.

It is widely acknowledged that the success of transfer learning comes from the knowledge in the pre-trained model. Considering that there are so many PTMs in a PTM hub, it is

appealing to transfer multiple PTMs simultaneously, a problem we call “*multiple PTMs tuning*”. Naturally, we expect multiple PTMs tuning can outperform single PTM tuning.

Unfortunately, multiple PTMs tuning is under-explored due to its technical difficulty. If multiple PTMs are homogeneous, *i.e.*, they share the same network architecture, the problem becomes easier. Researchers in this area focused on how to align and merge multiple PTMs. Singh and Jaggi (2020) defined transportation cost between neural representations and minimized the induced Wasserstein distance to align neurons from each PTM. Shu et al. (2021) developed a channel-wise alignment method dedicated to convolutional neural networks with a learnable gating function to merge multiple PTMs. Prior to this paper, Shu et al. (2021) held the state-of-the-art result in homogeneous PTMs tuning.

Heterogeneous PTMs tuning is much more difficult than homogeneous PTMs tuning. It is still an unanswered question due to the architectural heterogeneity among PTMs. In practice, however, this challenging problem is more important as pre-trained models in PTM hubs generally have different architectures and heterogeneity is common.

This paper tries to exploit PTM hubs as sufficiently as possible. In the proposed paradigm, PTMs are first ranked by LogME, then top-K ranked PTMs from the PTM hub are selected for multiple PTMs tuning. A Bayesian tuning method (B-Tuning, see Section 5.3) is further proposed to solve the multiple PTMs tuning problem. Excitingly, our method is capable of both homogeneous PTMs and heterogeneous PTMs. It fills the blank in heterogeneous PTMs tuning, and surpasses the state-of-the-art method (Shu et al., 2021) dedicated to homogeneous PTMs tuning.

3. Ranking pre-trained models

Ranking pre-trained models requires a transferability metric. But before introducing the transferability metric in Section 3.2, we need to know how to quantify its fidelity to the reference transferability performance, which is elaborated in the following Section 3.1.

3.1 How to measure the performance of a transferability metric?

A transfer learning task (in the form of a dataset $\mathcal{D} = \{(x_i, Y_i)\}_{i=1}^n$) should have an evaluation metric (accuracy, MAP, MSE, *etc.*) to measure the reference transfer performance T_k of fine-tuning ϕ_k with sufficient hyper-parameter tuning. A practical assessment method should produce a score S_k for each pre-trained model ϕ_k (ideally without fine-tuning ϕ_k on \mathcal{D}), and the scores $\{S_k\}_{k=1}^M$ should well correlate with $\{T_k\}_{k=1}^M$ so that top-performing pre-trained models can be selected by simply evaluating the scores $\{S_k\}_{k=1}^M$.

A perfect pre-trained model assessing method would produce $\{S_k\}_{k=1}^M$ with precisely the same order as $\{T_k\}_{k=1}^M$. To measure the deviation from the perfect method, we can use simple metrics like top-1 accuracy or top-K accuracy (whether the fraction among top-K in $\{S_k\}_{k=1}^M$ are also top-K in $\{T_k\}_{k=1}^M$). Nevertheless, top-1 accuracy is too conservative and top-K accuracy is not comparable across different values of M . Rank correlation (Fagin et al., 2003) is a good alternative to directly measure the correlation between $\{S_k\}_{k=1}^M$ and $\{T_k\}_{k=1}^M$. The prior work (Nguyen et al., 2020) adopted Pearson’s linear correlation coefficient, but neither Pearson’s linear correlation nor its variant (Spearman’s rank correlation) has a simple interpretation (see the interpretation of τ below). Therefore, they are not used in this paper.

The rank correlation method we choose is Kendall's τ coefficient (Kendall, 1938), which counts concordant pairs to capture the possibility of T_i being better than T_j if S_i is better than S_j in choosing a good pre-trained model.

Without loss of generality, we assume larger values of transfer performance T and score S are preferred (*e.g.*, accuracy). If this is not the case (*e.g.*, transfer performance is measured by mean square error and small values are favored), the negation $-T$ can be considered. For a pair of measures (T_i, S_i) and (T_j, S_j) , the pair is concordant if $T_i < T_j \wedge S_i < S_j$ or $T_i > T_j \wedge S_i > S_j$ (concisely speaking, $\text{sgn}(T_i - T_j)\text{sgn}(S_i - S_j) = 1$). The Kendall's τ coefficient is defined by the following equation, which enumerates all $\binom{M}{2}$ pairs and counts the number of concordant pairs minus the number of discordant pairs.

$$\tau = \frac{\sum_{1 \leq i < j \leq M} \text{sgn}(T_i - T_j)\text{sgn}(S_i - S_j)}{\binom{M}{2}}$$

How to interpret τ (Fagin et al., 2003): The range of τ is $[-1, 1]$. $\tau = 1$ means T and S are perfectly correlated ($S_i > S_j \iff T_i > T_j$), and $\tau = -1$ means T and S are reversely correlated ($S_i > S_j \iff T_i < T_j$). *If T and S have a correlation value of τ , the probability of $T_i > T_j$ is $\frac{\tau+1}{2}$ when $S_i > S_j$.*

Pay attention to top-performing models. Since a major application of transferability metric is to select top-performing pre-trained models, discordant/concordant pairs should be weighted more if T_i, T_j, S_i, S_j are larger. This can be taken care of by τ_w (Vigna, 2015), a weighted variant of Kendall's τ . The details of calculating τ_w can be found in the SciPy implementation. With the weighting scheme, correlation value τ_w corresponds to a proportion interval of concordant pairs rather than a unique proportion value $\frac{\tau_w+1}{2}$. Nevertheless, the interval lies near the value $\frac{\tau_w+1}{2}$. Therefore, we can roughly use the probability $\frac{\tau_w+1}{2}$ of concordant pairs to interpret correlation value τ_w .

In short, we measure the correlation between $\{S_k\}_{k=1}^M$ and $\{T_k\}_{k=1}^M$ by τ_w (Vigna, 2015). *Larger τ_w indicates a better correlation and better assessment.*

3.2 The LogME approach

This section describes LogME in detail. Since a transferability metric measures the transferability of pre-trained models, it should produce a score S_k for each PTM ϕ_k independent of the rest PTMs. We thus drop the subscript k in this section.

An important goal of designing transferability metrics is to quickly assess many PTMs. With that in mind, we set minimizing assessment time as a priority. First, to avoid expensive optimization of the whole PTM, PTM ϕ is regarded as a fixed feature extractor. Note that Nguyen et al. (2020) were limited to supervised pre-trained models because they used a pre-trained classification head h . In contrast, *we only use the pre-trained representation model ϕ so that the proposed method can be applied to any pre-trained model* (whether supervised pre-trained or unsupervised pre-trained).

With ϕ fixed, features $\{f_i = \phi(x_i)\}_{i=1}^n$ and labels $\{Y_i\}_{i=1}^n$ of the target task are what we can use to assess pre-trained models. The rest of this section discusses how to estimate the compatibility of features and labels as a transferability metric.

3.2.1 EVIDENCE CALCULATION

We first consider a simple case with D -dimensional features $f_i \in \mathbb{R}^D$ and scalar labels $y_i \in \mathbb{R}$. Note that the actual label Y_i can be non-scalar, and how to extend from scalar labels y_i to vector labels Y_i is explained in Section 3.2.2.

Let the feature matrix $F \in \mathbb{R}^{n \times D}$ denote all the features and $y \in \mathbb{R}^n$ denote all the labels. A direct measurement of the compatibility between features F and labels y is the probability density $p(y|F)$, which is intractable without a parameterized model. Since the rule-of-thumb transfer learning practice is to add a linear layer on top of the pre-trained model, we use a linear model upon features parameterized by w .

A straightforward approach to deal with the linear model is to find the best w^* by logistic or linear regression under maximum likelihood estimation, and to assess pre-trained models by the likelihood $p(y|F, w^*)$. However, it is well known that *maximum likelihood estimation is prone to over-fitting* (Bishop, 2006). Regularization techniques like L2 regularization may alleviate over-fitting at the cost of additional hyper-parameters, which requires manual intervention or grid search to tune those hyper-parameters. Even after extensive hyper-parameter tuning, its performance is not satisfying as observed in Section 6.6, because finding an optimal hyper-parameter is very difficult. *Ideally, a transferability metric should have no hyper-parameters so that it can be applied to downstream tasks without manual intervention.* Obviously, this approach does not satisfy the hyperparameter-free property.

The disadvantage of the above approach can be overcome by the evidence approach introduced below. Evidence (also known as marginalized likelihood) is defined as $p(y|F) = \int p(w)p(y|F, w)dw$, which integrates over all possible values of w rather than one w^* value. This evidence-based approach is an elegant model selection approach and has a rigorous theoretical foundation (Knuth et al., 2015). $p(w)$ and $p(y|F, w)$ are modeled by a graphical model (Figure 3) specified by two positive hyper-parameters α and β : the prior distribution of the weight is an isotropic multivariate Gaussian $w \sim \mathcal{N}(0, \alpha^{-1}I)$, and the distribution of each observation is a one-dimensional normal distribution $p(y_i|f_i, w, \beta) \sim \mathcal{N}(y_i|w^T f_i, \beta^{-1})$. Fortunately, hyper-parameters α and β can be automatically set to their optimal values as described in Section 3.2.2.

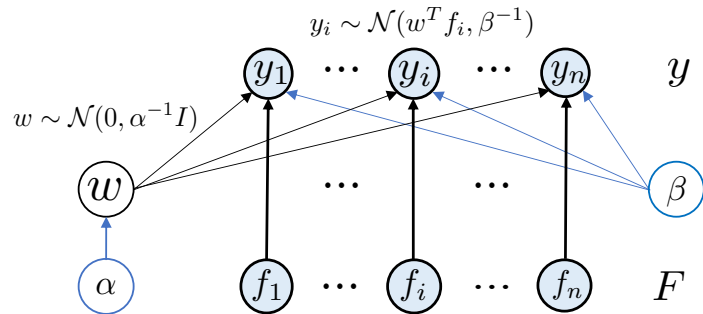


Figure 3: The directed graphical model for calculating evidence.

According to the causal structure in Figure 3 and the basic principles in graphical models (Koller and Friedman, 2009), the evidence can be calculated analytically as follows:

$$p(y|F, \alpha, \beta) = \int p(w|\alpha) \prod_{i=1}^n p(y_i|f_i, w, \beta) dw = (\frac{\beta}{2\pi})^{\frac{n}{2}} (\frac{\alpha}{2\pi})^{\frac{D}{2}} \int e^{-\frac{\alpha}{2}w^T w - \frac{\beta}{2}\|Fw - y\|^2} dw. \quad (1)$$

Equation 1 can be simplified by the identity $\int e^{-\frac{1}{2}(w^T A w + b^T w + c)} dw = \sqrt{\frac{(2\pi)^D}{|A|}} e^{-\frac{1}{2}c + \frac{1}{8}b^T A^{-1} b}$. Taking the logarithm to make the equation simple, Equation 2 shows the logarithm of the evidence \mathcal{L} as a function of α, β , where $A = \alpha I + \beta F^T F, m = \beta A^{-1} F^T y$.

$$\mathcal{L}(\alpha, \beta) = \log p(y|F, \alpha, \beta) = \frac{n}{2} \log \beta + \frac{D}{2} \log \alpha - \frac{n}{2} \log 2\pi - \frac{\beta}{2} \|Fm - y\|_2^2 - \frac{\alpha}{2} m^T m - \frac{1}{2} \log |A| \quad (2)$$

3.2.2 EVIDENCE MAXIMIZATION AND LOGME

An unresolved issue in Equation 2 is how to choose α, β . Gull (1989) suggested choosing α, β to maximize the evidence, *i.e.*, use $(\alpha^*, \beta^*) = \arg \max_{\alpha, \beta} \mathcal{L}(\alpha, \beta)$. Because m and A are coupled, it is a difficult problem to directly maximize $\mathcal{L}(\alpha, \beta)$. Fortunately, MacKay (1992) proposed a heuristic algorithm to solve the maximization problem: (1) set initial value of α, β ; (2) evaluate A, m, γ with given α, β : $A = \alpha I + \beta F^T F, m = \beta A^{-1} F^T y, \gamma = \sum_{i=1}^D \frac{\beta \sigma_i^2}{\alpha + \beta \sigma_i^2}$, where σ_i are singular values of F ; (3) maximize α, β by solving $\frac{\partial \mathcal{L}}{\partial \alpha} = 0, \frac{\partial \mathcal{L}}{\partial \beta} = 0$ with m, γ fixed, which yields $\alpha \leftarrow \frac{\gamma}{m^T m}, \beta \leftarrow \frac{n - \gamma}{\|Fm - y\|_2^2}$. The algorithm is called MacKay's algorithm (Algorithm 2), and has been heuristic as of its invention by MacKay (1992). Section 4.1 gives the first theoretical analysis for the convergence guarantee. Interestingly, the fixed point iteration used for the convergence analysis brings a new and faster algorithm for evidence maximization (Algorithm 3). Please refer to Section 4.1 for details.

After the convergence of evidence maximization, the logarithm maximum evidence $\mathcal{L}(\alpha^*, \beta^*)$ is used to evaluate the compatibility between features and labels. Because $\mathcal{L}(\alpha^*, \beta^*)$ scales linearly with n , we normalize it as $\frac{\mathcal{L}(\alpha^*, \beta^*)}{n}$ and term it **LogME** (logarithm of maximum evidence). Discussion on the influence of dimensionality D is presented in Section 4.2. LogME can be intuitively interpreted as the logarithm of maximum label evidence given pre-trained features.

Extending LogME to complex cases. The LogME approach starts from a single-target regression. If the target problem is a multivariate regression task, *i.e.*, $Y \in \mathbb{R}^{n \times C}$, we can calculate LogME for each dimension c ($1 \leq c \leq C$) and average them over the C dimension. If the target problem is a classification task with C classes, Equation 1 cannot be calculated analytically (Daunizeau, 2017) with a categorical prior distribution. State-of-the-art approximation methods like Laplace approximation (Immer et al., 2021) work well in toy data, but perform unsatisfyingly in realistic tasks, as mentioned later in Section 6.1. Therefore, we turn to an alternative solution: convert the classification labels to one-hot labels and treat the problem as multivariate regression. This approach also works for multi-label classification as well. This way, LogME can be used in both (single-label and multi-label) classification and regression tasks.

The overall algorithm of LogME is described in Algorithm 1.

3.2.3 COMPUTATIONAL SPEEDUP

Although the Bayesian approach of maximum evidence has a rigorous theoretical explanation (Knuth et al., 2015), it inherits the drawback of Bayesian methods with high computational complexity. A naïve implementation with Algorithm 2 results in a total complexity of $\mathcal{O}(CD^3 + nCD^2)$. For typical usage with $D \approx 10^3, n \approx 10^4, C \approx 10^3$, the computational cost is 10^{13} , with the wall-clock time comparable to fine-tuning PTM ϕ .

Algorithm 1 LogME

- 1: **Input:** Pre-trained model ϕ and target dataset $\mathcal{D} = \{(x_i, Y_i)\}_{i=1}^n$
- 2: **Output:** Logarithm of Maximum Evidence (LogME)
- 3: Extract features using pre-trained model ϕ : $F \in \mathbb{R}^{n \times D}$, $f_i = \phi(x_i)$, $Y \in \mathbb{R}^{n \times C}$
- 4: Compute SVD of F : $F = U\Sigma V^T$. Then $F^T F = V \text{diag}\{\sigma^2\} V^T$
- 5: **for** dimension $c = 1$ to C **do**
- 6: Let $y = Y^{(c)} \in \mathbb{R}^n$,
- 7: Calculate the LogME value \mathcal{L}_c by evidence maximization (Algorithm 2 or Algorithm 3).
- 8: **end for**
- 9: Return LogME $\frac{1}{C} \sum_{c=1}^C \mathcal{L}_c$

Algorithm 2 Evidence Maximization by MacKay's Algorithm

- 1: **Input:** Extracted features $F \in \mathbb{R}^{n \times D}$ and corresponding labels $y \in \mathbb{R}^n$
- 2: **Output:** Logarithm of Maximum Evidence (LogME)
- 3: **Note:** F has been pre-decomposed into $F = U\Sigma V^T$
- 4: Initialize $\alpha = 1, \beta = 1$
- 5: **while** α, β not converge **do**
- 6: Compute $\gamma = \sum_{i=1}^D \frac{\beta \sigma_i^2}{\alpha + \beta \sigma_i^2}, \Lambda = \text{diag}\{(\alpha + \beta \sigma^2)\}$
- 7: **Naïve:** $A = \alpha I + \beta F^T F, m = \beta A^{-1} F^T y$
- 8: **Optimized** by You et al. (2021): $m = \beta(V(\Lambda^{-1}(V^T(F^T y))))$
- 9: Update $\alpha \leftarrow \frac{\gamma}{m^T m}, \beta \leftarrow \frac{n - \gamma}{\|Fm - y\|_2^2}$
- 10: **end while**
- 11: Compute and return $\mathcal{L} = \frac{1}{n} \mathcal{L}(\alpha, \beta)$ using Equation 2

Algorithm 3 Evidence Maximization by Optimized Fixed Point Iteration

- 1: **Input:** Extracted features $F \in \mathbb{R}^{n \times D}$ and corresponding labels $y \in \mathbb{R}^n$
- 2: **Output:** Logarithm of Maximum Evidence (LogME)
- 3: **Require:** Truncated SVD of F : $F = U_r \Sigma_r V_r^T$, with $U_r \in \mathbb{R}^{n \times r}, \Sigma_r \in \mathbb{R}^{r \times r}, V_r \in \mathbb{R}^{D \times r}$.
- 4: **Compute** the first r entries of $z = U_r^T y$
- 5: **Compute** the sum of remaining entries $\Delta = \sum_{i=r+1}^n z_i^2 = \sum_{i=1}^n y_i^2 - \sum_{i=1}^r z_i^2$
- 6: Initialize $\alpha = 1, \beta = 1, t = \frac{\alpha}{\beta} = 1$
- 7: **while** t not converge **do**
- 8: Compute $m^T m = \sum_{i=1}^r \frac{\sigma_i^2 z_i^2}{(t + \sigma_i^2)^2}, \gamma = \sum_{i=1}^r \frac{\sigma_i^2}{t + \sigma_i^2}, \|Fm - y\|_2^2 = \sum_{i=1}^r \frac{z_i^2}{(1 + \sigma_i^2/t)^2} + \Delta$
- 9: Update $\alpha \leftarrow \frac{\gamma}{m^T m}, \beta \leftarrow \frac{n - \gamma}{\|Fm - y\|_2^2}, t = \frac{\alpha}{\beta}$
- 10: **end while**
- 11: Compute $m = V_r \Sigma' z$, where $\Sigma'_{ii} = \frac{\sigma_i}{t + \sigma_i^2} (1 \leq i \leq r)$.
- 12: Compute and return $\mathcal{L} = \frac{1}{n} \mathcal{L}(\alpha, \beta)$ using Equation 2

Our conference paper (You et al., 2021) accelerated the computation by avoiding matrix inversion and matrix-matrix multiplication, as shown in Line 8 of Algorithm 2. In this paper, we present a convergence analysis of the MacKay’s algorithm by fixed point iteration. It turns out that the analysis implies a faster algorithm for evidence maximization. The algorithm is presented in Algorithm 3 and its rationale is explained in Section 4.1.

Table 2: The complexity of Algorithm 1 with three implementations of evidence maximization. n, C are the number of samples and the number of classes in classification (or the number of target variables in regression) in downstream tasks, and D is the dimension of features produced by a pre-trained model.

Evidence maximization method	Complexity per while-loop	Overall complexity
naïve implementation	$\mathcal{O}(D^3 + nD^2)$	$\mathcal{O}(nCD^2 + CD^3)$
optimized by You et al. (2021)	$\mathcal{O}(D^2 + nD)$	$\mathcal{O}(nD^2 + nCD + CD^2 + D^3)$
fixed point iteration (this paper)	$\mathcal{O}(n)$	$\mathcal{O}(nD^2 + nCD)$

Table 2 compares the complexity of calculating LogME with three implementations of evidence maximization. The naïve implementation is biquadratic, You et al. (2021) made it cubic, and this paper further reduces the number of cubic terms. The optimized algorithm makes a time-consuming Bayesian approach fast enough, reducing the wall-clock time by order of 10^2 (see Section 6.5 for a quantitative measurement). Note that three implementation methods are functionally equivalent and only differ in computational complexity. Therefore, *the fixed point iteration proposed in this paper is used by default in our implementation.*

4. Theoretical analyses of LogME

In this section, we analyze two theoretical aspects of the proposed LogME, which further explains the rationality behind the LogME algorithm and why LogME works.

4.1 Convergence analysis of evidence maximization

Historical remarks: The evidence maximization procedure in Section 3.2.2 was firstly proposed by MacKay (1992) as a heuristic method to maximize the evidence of given data, following the spirit of empirical Bayesian learning (Bishop, 1995). Its theoretical analysis is missing and it remains heuristic in modern machine learning textbooks like Murphy (2012). In 2016, researchers (Li et al., 2016) revealed that if the predictive uncertainty β is known, the maximization over model uncertainty α can be viewed as a special instantiation of the EM algorithm (Dempster et al., 1977). However, pre-determining β is suboptimal, and in practice α, β are simultaneously maximized. To the best of our knowledge, we are the first to analyze the MacKay’s algorithm when α, β are simultaneously optimized.

For the convenience of readers, we collect necessary notations here: n is the number of data examples; D is the size of feature dimensionality; $F \in \mathbb{R}^{n \times D}$ is the feature matrix, with $r = \text{rank}(F)$ being its rank; $y \in \mathbb{R}^n$ is the label vector of data examples. We can immediately get $r \leq \min\{n, D\}$.

The key in our analysis is to take full advantage of the singular value decomposition of the feature matrix $F = U\Sigma V^T$, where $U \in \mathbb{R}^{n \times n}$, $V \in \mathbb{R}^{D \times D}$, and $\Sigma \in \mathbb{R}^{n \times D}$. Note that Σ only has r non-zero entries: $\Sigma_{ii} = \sigma_i > 0$ ($1 \leq i \leq r$) where σ_i^2 is the i -th largest eigenvalue of $F^T F$ and $\sigma_i = 0$ ($r+1 \leq i \leq \max(n, D)$). To simplify the expression, let $z = U^T y$ be the transformed y under orthogonal bases U , *i.e.*, $y = Uz$.

The MacKay's algorithm (Algorithm 2) consists of a while-loop. The key to analyzing the whole algorithm is to analyze each iteration of the while-loop, which is listed in Algorithm 4 for readers' convenience. During each iteration, new values α', β' are computed based on old values α, β , which can be regarded as evaluating a vector-valued function $(\alpha', \beta') = g(\alpha, \beta)$.

Algorithm 4 One iteration of evidence maximization in Algorithm 2.

- 1: Input: α, β ; Output: α', β' for the next iteration.
- 2: Compute $A = \alpha I + \beta F^T F$, $m = \beta A^{-1} F^T y$, $\gamma = \sum_{i=1}^D \frac{\beta \sigma_i^2}{\alpha + \beta \sigma_i^2}$
- 3: Return $\alpha' = \frac{\gamma}{m^T m}$, $\beta' = \frac{n - \gamma}{\|Fm - y\|_2^2}$

The MacKay's algorithm converges if and only if $(\alpha', \beta') = (\alpha, \beta)$ in Algorithm 4. With F, y as constants, the convergence of Algorithm 2 is equivalent to the existence of the fixed point of the vector-valued function g , *i.e.*, the existence of α, β such that $(\alpha, \beta) = g(\alpha, \beta)$.

In general, fixed points of vector-valued functions are difficult to analyze and visualize. Fortunately, we find that the vector-valued function $(\alpha', \beta') = g(\alpha, \beta)$ is homogeneous: $g(k\alpha, k\beta) = kg(\alpha, \beta), \forall k > 0$. Let $t = \alpha/\beta$, and $t' = \alpha'/\beta'$, the vector-valued function $(\alpha', \beta') = g(\alpha, \beta)$ induces a scalar function $t' = f(t)$, whose explicit form can be derived in Theorem 1. Evaluating $g(\alpha, \beta)$ is equivalent to calculating $f(\frac{\alpha}{\beta})$, which is easier to analyze.

Theorem 1 Algorithm 4 induces a scalar function (Equation 3) with $t = \frac{\alpha}{\beta}$ and $t' = \frac{\alpha'}{\beta'}$.

$$t' = f(t) = \left(\frac{n}{n - \sum_{i=1}^D \frac{\sigma_i^2}{t + \sigma_i^2}} - 1 \right) t^2 \frac{\sum_{i=1}^n \frac{z_i^2}{(t + \sigma_i^2)^2}}{\sum_{i=1}^n \frac{\sigma_i^2 z_i^2}{(t + \sigma_i^2)^2}} \quad (3)$$

The proof is in Appendix B. Although $f(t)$ seems very complicated and completely understanding its behavior is difficult, surprisingly, the existence of $f(t)$'s fixed point can be guaranteed with an interpretable condition, which is presented in the following Theorem 2.

Theorem 2 If $r < n$ and $\sum_{1 \leq i, j \leq n} (z_i^2 - z_j^2)(\sigma_i^2 - \sigma_j^2) > 0$, then $f(t)$ has a fixed point and thus the MacKay's algorithm will converge.

The proof is in Appendix C. Theorem 2 requires two conditions to guarantee the fixed point: $r < n$ and $\sum_{1 \leq i, j \leq n} (z_i^2 - z_j^2)(\sigma_i^2 - \sigma_j^2) > 0$. The first condition is easy to interpret and can be easily satisfied: usually $n > D$, and $n > D \geq r$ naturally holds. The condition $\sum_{1 \leq i, j \leq n} (z_i^2 - z_j^2)(\sigma_i^2 - \sigma_j^2) > 0$ is new in this paper. Note that $z = U^T y$ and $z_i = U_i^T y$, where U_i (the i -th column of U) is the left-singular vector of the singular value σ_i , which means that z_i is the projection of label vector y in the direction of the left-singular vector for the singular value σ_i . Intuitively speaking, $\sum_{1 \leq i, j \leq n} (z_i^2 - z_j^2)(\sigma_i^2 - \sigma_j^2) > 0$ requires z_i^2

to share roughly the same descending order as σ_i^2 . For larger σ_i^2 (*i.e.*, smaller i), it means the projection of y in the corresponding left-singular vector should be larger, which can be interpreted as a rigorous way to say that *labels y are meaningful with respect to the features F*. We would like to emphasize that the requirement on the order of z_i^2 is *soft*: strict order $z_i^2 \geq z_j^2 \iff i \leq j \iff \sigma_i^2 \geq \sigma_j^2$ certainly assures the convergence condition $\sum_{1 \leq i, j \leq n} (z_i^2 - z_j^2)(\sigma_i^2 - \sigma_j^2) > 0$, but as long as most z_i^2 follow the order, the condition can be satisfied. We find that all experiments in this paper admit the convergence condition, *i.e.*, the evidence maximization algorithm is guaranteed to converge if the data is meaningful. For example, Figure 4 plots $f(t)$ on the CIFAR10 dataset, which clearly shows cross points of $f(t)$ and t , so the convergence condition $\sum_{1 \leq i, j \leq n} (z_i^2 - z_j^2)(\sigma_i^2 - \sigma_j^2) > 0$ holds.

Make the fixed point iteration faster. Note that the fixed point iteration Equation 3 requires explicitly computing $z = U^T y$ with $\mathcal{O}(n^2)$ storage and computation, which would be undesired if n is very large. To make it a practical algorithm, we take advantage of the fact that $\sigma_i = 0$ for $i > r$, and optimize the fixed point iteration as follows:

$$\begin{aligned} t' = f(t) &= \left(\frac{n}{n - \sum_{i=1}^D \frac{\sigma_i^2}{t + \sigma_i^2}} - 1 \right) t^2 \frac{\sum_{i=1}^n \frac{z_i^2}{(t + \sigma_i^2)^2}}{\sum_{i=1}^n \frac{\sigma_i^2 z_i^2}{(t + \sigma_i^2)^2}} \\ &= \left(\frac{n}{n - \sum_{i=1}^r \frac{\sigma_i^2}{t + \sigma_i^2}} - 1 \right) t^2 \frac{\sum_{i=1}^r \frac{z_i^2}{(t + \sigma_i^2)^2} + \frac{1}{t^2} \sum_{i=r+1}^n z_i^2}{\sum_{i=1}^r \frac{\sigma_i^2 z_i^2}{(t + \sigma_i^2)^2}} \\ &= \left(\frac{n}{n - \sum_{i=1}^r \frac{\sigma_i^2}{t + \sigma_i^2}} - 1 \right) t^2 \frac{\sum_{i=1}^r \frac{z_i^2}{(t + \sigma_i^2)^2} + \frac{1}{t^2} (\sum_{i=1}^n y_i^2 - \sum_{i=1}^r z_i^2)}{\sum_{i=1}^r \frac{\sigma_i^2 z_i^2}{(t + \sigma_i^2)^2}} \end{aligned}$$

Therefore, we can derive a faster algorithm (Equation 4) for the fixed point iteration, which only requires the first r entries of z without computing the full U matrix or the full z vector. This is the exact algorithm we implement in Algorithm 3.

$$t' = f(t) = \left(\frac{n}{n - \sum_{i=1}^r \frac{\sigma_i^2}{t + \sigma_i^2}} - 1 \right) t^2 \frac{\sum_{i=1}^r \frac{z_i^2}{(t + \sigma_i^2)^2} + \frac{1}{t^2} (\sum_{i=1}^n y_i^2 - \sum_{i=1}^r z_i^2)}{\sum_{i=1}^r \frac{\sigma_i^2 z_i^2}{(t + \sigma_i^2)^2}} \quad (4)$$

4.2 Influence of dimensionality

In Section 3.2.2, we normalize the LogME value by the number of examples because Equation 2 scales linearly with n . The influence of feature dimension D is, however, unclear. In this section, we find two cases (feature duplicate and feature padding) where *LogME value remains unchanged when the feature dimension goes up without introducing more information*. The two cases show the existence of infinitely many features with arbitrary feature dimensions that share the same LogME value, therefore canceling the necessity of dimensionality normalization.

Corollary 3 (feature duplicate) LogME value will remain the same if the feature consists of arbitrary replicas of the original feature. Formally speaking, if the LogME value for

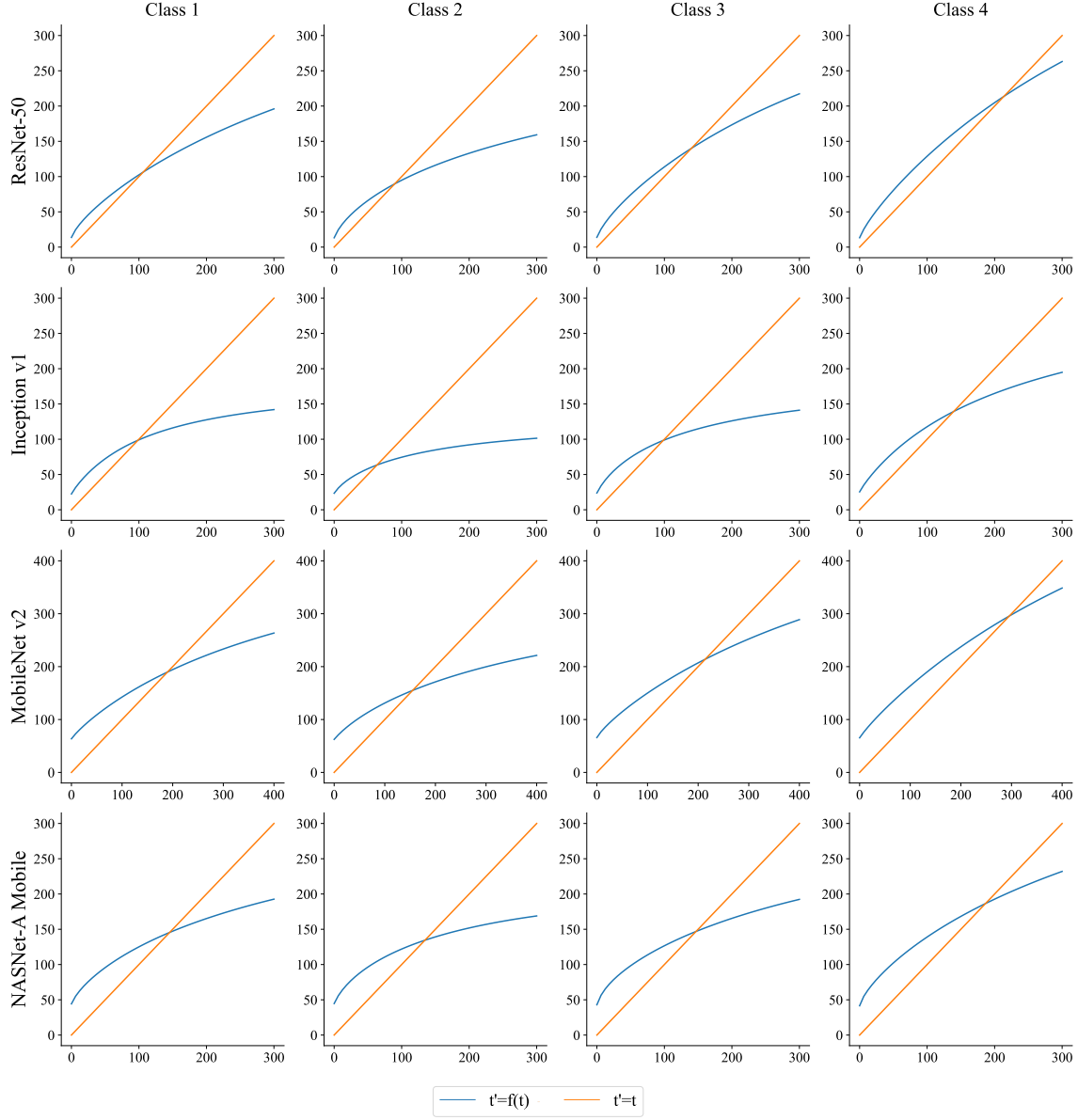


Figure 4: Fixed points of $f(t)$ in Equation 3 for the first 4 classes in CIFAR10 with 4 pre-trained models. The full figure for all the 10 classes in CIFAR10 with 5 pre-trained models can be found in Figure 13, which is omitted here to prettify the layout. We plot $t' = f(t)$ (in blue) and $t' = t$ (in orange), whose intersections are fixed points $f(t) = t$. The existence of fixed points guarantees the convergence of the MacKay's algorithm for evidence maximization.

$F \in \mathbb{R}^{n \times D}$ and $y \in \mathbb{R}^n$ is \mathcal{L} , then the LogME value for $\tilde{F} = [F, \dots, F] \in \mathbb{R}^{n \times qD}$ and $y \in \mathbb{R}^n$ is also \mathcal{L} . ($q \in \mathbb{N}$ is a natural number to represent the number of replicas.)

Corollary 4 (feature padding) LogME value will remain the same if the feature is padded with an arbitrary number of zeros. Formally speaking, if the LogME value for $F \in \mathbb{R}^{n \times D}$ and $y \in \mathbb{R}^n$ is \mathcal{L} , then the LogME value for $\tilde{F} = [F, \mathbf{0}] \in \mathbb{R}^{n \times (D+d)}$ and $y \in \mathbb{R}^n$ is also \mathcal{L} . ($d \in \mathbb{N}$ is a natural number and $\mathbf{0} \in \mathbb{R}^{n \times d}$ is a matrix with all zero entries.)

The proofs of Corollary 3 and Corollary 4 are in Appendix D and Appendix E, respectively. The core idea is to find the closed-form relationship between decompositions of \tilde{F} and F .

Corollary 3 and Corollary 4 imply that duplicating features or padding features with zeros will not change the value of LogME. LogME is capable of filtering out redundant information in features, explaining its excellent empirical performance in You et al. (2021).

5. Tuning pre-trained models

The new paradigm we propose consists of ranking and tuning pre-trained models. Sections 3 and 4 described technical details in ranking pre-trained models, including the transferability metric LogME and its theoretical analyses. This section starts to focus on tuning pre-trained models, completing the rest part of the new paradigm.

We identify two possible scenarios of tuning pre-trained models: single best PTM tuning and multiple PTMs tuning. (1) *Single best PTM tuning* is suitable if there are no constraints on the network architecture, parameter count, or FLOPs of computation. These constraints are common in industrial applications, but are less important in academic research. Therefore, single best PTM tuning is common in academic research. Intuitively, the rest PTMs are inferior to the best ranked PTM so they would not help much. We refer readers to dedicated papers (Chen et al., 2019; Kou et al., 2020; You et al., 2020) on how to fine-tune a single PTM, which is not the focus of this paper. (2) When we deploy neural networks in industrial applications, typically there are strict constraints on the budget of memory footprint or power consumption. Therefore, the pre-trained model ϕ_t satisfying these constraints is probably not the best ranked. Before this paper, practitioners could only fine-tune ϕ_t , and the knowledge of the PTM hub $\{\phi_i\}_{i=1}^M$ cannot be exploited. In this paper, we show that it is possible to transfer knowledge from several teacher PTMs $\{\phi_k\}_{k=1}^K$ to the target pre-trained model ϕ_t during fine-tuning, which we call “multiple PTMs tuning”.

A side issue of tuning multiple PTMs is how to select the teacher PTMs. Typically, $K < M$, *i.e.*, not all PTMs are necessary, since some PTMs may not be suitable for the target task and would hinder the transfer learning procedure. However, for M pre-trained models, the possible number of teacher combinations is $\mathcal{O}(2^M)$, which is impractical to enumerate. To overcome the exponential complexity, the PTM ranking can come to the rescue. With the PTM ranking, we can greedily select teacher PTMs following the rank. For example, if we want to choose K teacher PTMs, then the top- K ranked PTMs $\{\phi_k\}_{k=1}^K$ are the teacher of knowledge transfer. As for how to choose the hyper-parameter K ($1 \leq K \leq M$), we give empirical guidelines in Section 6.3.

Multiple PTMs tuning offers a unique advantage over simply fine-tuning the target pre-trained model ϕ_t : if the specified target pre-trained model ϕ_t is not the best-ranked, we can still improve it by transferring knowledge from top-performing PTMs $\{\phi_k\}_{k=1}^K$.

5.1 Problem setup of multiple PTMs tuning

Now suppose we have selected K pre-trained models $\{\phi_k\}_{k=1}^K$, with each pre-trained model ϕ_k transforming input x into a D_k dimensional feature vector. In general, pre-trained models $\{\phi_k\}_{k=1}^K$ have various network architectures, and dimensionality of features $\{D_k\}_{k=1}^K$ can vary. Let ϕ_t be the target architecture, which transforms the input into D_t dimensional feature vector. Formally, the multiple PTMs tuning problem is to fine-tune a pre-trained model ϕ_t by leveraging selected pre-trained models $\{\phi_k\}_{k=1}^K$, as shown in Figure 2.

To fine-tune a model ϕ_t in a target task, a new output head would be attached after ϕ_t , where target-specific loss is calculated. The target-specific head and loss are necessary for every possible solution to multiple PTMs tuning, which is taken cared of by a loss function L_{task} . We will not elaborate on L_{task} as it varies with tasks. Next we summarize existing approaches to the problem in Section 5.2 and introduce our method in Section 5.3.

5.2 Existing approaches to the problem of multiple PTMs tuning

A baseline approach is to fine-tune ϕ_t without considering teacher PTMs $\{\phi_k\}_{k=1}^K$. This can serve as a baseline to measure the improvement brought by multiple PTMs tuning.

The knowledge distillation approach to multiple PTMs tuning is knowledge distillation (Hinton et al., 2015) in the feature space via mean-square error. Since the feature dimensions between ϕ_t and $\{\phi_k\}_{k=1}^K$ may be different, a transformation module is necessary. The knowledge distillation (KD) method takes advantage of selected pre-trained models by adding a regularization term $L_{KD} = \frac{1}{n} \sum_{i=1}^n \frac{1}{K} \sum_{k=1}^K \|\phi_k(x_i) - W_k \phi_t(x_i)\|_2^2$, where W_k is learnable parameter to transform D_t dimensional feature $\phi_t(x_i)$ into D_k dimensional vector compatible with $\phi_k(x_i)$. Even if $D_k = D_t$, the semantic of each dimension in ϕ_t and ϕ_k may vary, making it necessary to introduce the transformation parameter W_k . The final loss is $L_{task} + \lambda L_{KD}$, with hyper-parameter λ trading two terms. The KD method is another simple but general baseline in multiple PTM tuning. It can be applied to various PTMs but the performance improvement is limited.

Zoo-tuning for homogeneous PTMs tuning. In the special case when ϕ_t and $\{\phi_k\}_{k=1}^K$ all share the same network architecture, Zoo-tuning proposed by Shu et al. (2021) adaptively aggregates parameters of $\{\phi_k\}_{k=1}^K$ into ϕ_t in a layer-wise fashion. It does not modify the loss L_{task} , but changes the training process by model aggregation. Zoo-tuning is the current state-of-the-art method for homogeneous PTMs tuning, but it fails to deal with the heterogeneous scenario when architectures of ϕ_t and $\{\phi_k\}_{k=1}^K$ are different.

5.3 B-Tuning: A Bayesian approach to multiple PTMs tuning

We draw lessons from the shortcomings of the aforementioned knowledge distillation approach and the Zoo-tuning approach. Knowledge distillation operates at the level of output features, which works for heterogeneous PTMs but aligning features across PTMs is not easy. Zoo-tuning operates at the level of parameters (layers), thereby limiting itself in the homogeneous case. Taking advantages from both sides, our approach should operate at the level of features to hide the heterogeneity among PTMs, and should go beyond features to avoid explicitly aligning features from various pre-trained models. Inspired by the ranking metric

(LogME), we propose a B-Tuning approach with the help of posterior predictive distribution in Bayesian regression.

Posterior predictive distribution is $p(y'|f, F, y) = \int_w p(y'|w, f)p(w|F, y)dw$, which predicts the label y' of incoming feature f conditioned on all the available training features F and labels y rather than just using f . With pre-computed α^*, β^*, m (byproducts of the LogME algorithm), $p(y'|w, f) \sim \mathcal{N}(w^T f, \beta^{*-1})$ by definition, and $p(w|F, y) = \frac{p(w)p(F, y|w)}{\int_{w'} p(w')p(F, y|w')dw'}$ by the Bayesian rule. Rasmussen (2003) show that $p(w|F, y) \sim \mathcal{N}(\beta^* A^{-1} F^T y, A^{-1})$ with $A = \alpha^* I + \beta^* F^T F$. Plugging in the distributions of $p(y'|w, f)$ and $p(w|F, y)$, Rasmussen (2003) show that $p(y'|f, F, y) \sim \mathcal{N}(f^T m, f^T A^{-1} f + \beta^{*-1})$ with $m = \beta^* A^{-1} F^T y$. In short, for extracted features $F \in \mathbb{R}^{n \times D}$ and labels $y \in \mathbb{R}^n$, the LogME algorithm gives α^*, β^*, m , and the posterior predictive distribution is $p(y'|f, F, y) \sim \mathcal{N}(f^T m, f^T A^{-1} f + \beta^{*-1})$. The derivation details of posterior predictive distribution can be found in Rasmussen (2003).

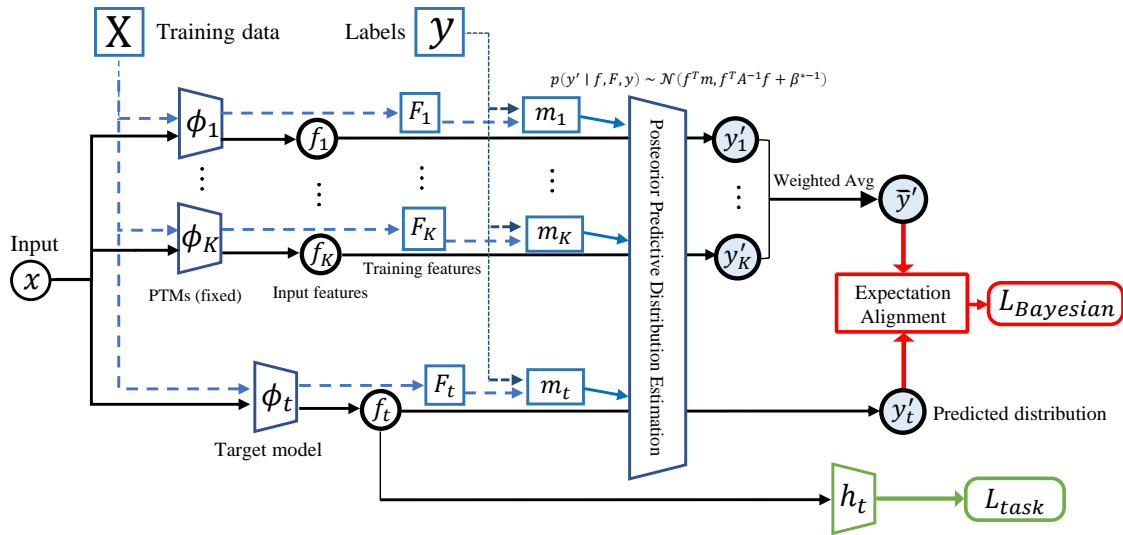


Figure 5: Illustration of B-Tuning. Dashed lines are pre-calculated before tuning.

Posterior predictive distribution depends on the training data (F, y) and incoming feature f . Let F_k be features extracted by the pre-trained model ϕ_k , $f_k = \phi_k(x)$ be the output feature of the current data point extracted by the pre-trained model ϕ_k , then each pre-trained model can produce a posterior predictive distribution $p(y'_k | f_k, F_k, y) \sim \mathcal{N}(f_k^T m_k, f_k^T A_k^{-1} f_k + \beta_k^{*-1})$. How to combining these distributions? We propose to mix them according to their LogME values $\{\mathcal{L}_k\}_{k=1}^K$ as mixture of Gaussians $\bar{y}' = \sum_{k=1}^K \pi_k y'_k$ where $\pi_k = \frac{\exp(\mathcal{L}_k/t)}{\sum_{j=1}^K \exp(\mathcal{L}_j/t)}$ and t is the temperature hyper-parameter (Hinton et al., 2015) that can be adjusted according to the difference of LogME values. Although $\{y'_k\}_{k=1}^K$ admit simple Gaussian distributions, the exact distribution of mixed \bar{y}' is untractable because features F_k come from the same dataset and $\{y'_k\}_{k=1}^K$ are dependent. Nevertheless, according to the linearity property of expectation, $\mathbb{E}\bar{y}' = \sum_{k=1}^K \pi_k \mathbb{E}y'_k = \sum_{k=1}^K \pi_k f_k^T m_k$, the expectation of \bar{y}' is known.

For the target model ϕ_t , the posterior predictive distribution is defined as $p(y'_t | f_t, F_t, y) \sim \mathcal{N}(f_t^T m_t, f_t^T A_t^{-1} f_t + \beta_t^{*-1})$. Since \bar{y}' can be regarded as prior knowledge from pre-trained models $\{\phi_k\}_{k=1}^K$, we can align the expectation of y'_t and \bar{y}' as a regularization term $L_{Bayesian} =$

$\frac{1}{n} \sum_{i=1}^n \|\mathbb{E}\bar{y}' - \mathbb{E}y'_t\|_2^2$. Note that the expectation is taken over the predictive distributions and can be calculated analytically. Extending the formula to multiple classes, the final expression of the regularization term is

$$L_{Bayesian} = \frac{1}{n} \sum_{i=1}^n \frac{1}{C} \sum_{c=1}^C \left(\sum_{k=1}^K \pi_k f_k^T m_{k,c} - f_t^T m_{t,c} \right)^2, \quad (5)$$

where $m_{k,c}, m_{t,c}$ are calculated by the LogME algorithm and are fixed during training. The final loss would be $L_{task} + \lambda L_{Bayesian}$, with λ to trade-off two terms. Because the method depends on the Bayesian approach of calculating posterior predictive distribution, we call it Bayesian Tuning, or **B-Tuning**. Figure 5 describes the method and the computation graph. Only ϕ_t is updated during B-Tuning while the teacher PTMs $\{\phi_k\}_{k=1}^K$ are fixed.

B-Tuning has two advantages over previous methods. (1) It hides the heterogeneity among PTMs by operating at the level of features, characterizing itself as a *general* solution to multiple PTMs tuning in both homogeneous and heterogeneous cases. (2) Despite its heavy mathematical derivation, B-Tuning has a simple interpretation: it aligns features adaptively with m serving as an attention-like mechanism, canceling the necessity of learning to transform features into a shared space like the knowledge distillation approach. The superiority of B-Tuning in multiple PTMs tuning is empirically demonstrated in Section 6.3.

6. Experiments

This paper presents comprehensive experiments. Section 6.1 illustrates the behavior of LogME on toy problems. Experiments on ranking PTMs and tuning PTMs are in Section 6.2 and Section 6.3 respectively, demonstrating the power of the proposed new paradigm. Section 6.5 quantitatively measures the efficiency of LogME and Section 6.6 compares LogME against a common approach of re-training head over a fixed feature extractor, providing a comprehensive understanding of LogME. Original data for some figures are available in the appendix. Code for LogME is available at <https://github.com/thuml/LogME>.

6.1 Illustration with toy data

To give readers an intuitive sense of how LogME works, we generate features with increasing noise to mimic the features extracted by pre-trained models with decreasing transferability and to check if LogME can measure the quality of features.

For classification (Figure 6 left), three clusters in a 2-D plane are generated, with colors representing the categories. Initially, the features are well separable so LogME has a large value. Then we add Gaussian noise with increasing variance to the data and the clustering structure in feature space disappears, leading to smaller LogME values as expected.

For regression (Figure 6 right), x is uniformly distributed ($x \sim \mathcal{U}[0, 1]$) and the output $y = 2x + \epsilon$ with observation error $\epsilon \sim \mathcal{N}(0, 0.1^2)$. By adding noise to the feature $x' = x + \mathcal{N}(0, t^2)$, the quality of feature x' becomes worse and it is harder to predict y from x' . With larger t (the standard deviation of noise), LogME becomes smaller as expected.

These toy experiments on synthesized data show that LogME is a good measure of the feature quality, and therefore can provide a good ranking for PTMs in a pre-trained model hub. The solid theoretical foundation behind LogME also brings an effective B-Tuning

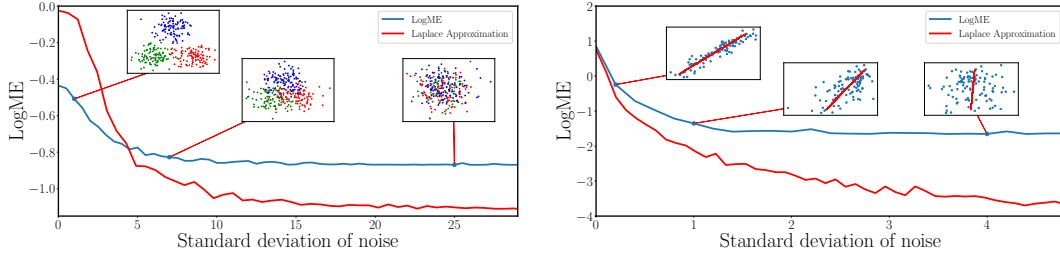


Figure 6: Toy data show that LogME value goes down with decreasing feature quality. Laplace Approximation means the LogME value calculated by Immer et al. (2021) using Laplace approximation.

method for multiple PTMs tuning. Together they make LogME a central technique in the new paradigm of ranking and tuning pre-trained models.

Figure 6 also shows the LogME value calculated by Immer et al. (2021) using Laplace approximation. In this toy experiment, both LogME and Laplace approximation correctly measure the trend of feature quality. In regression, the Laplace Approximation is strictly lower than LogME; in classification, Laplace approximation uses a categorical prior and approximates the marginal likelihood, while LogME converts classification labels to one-hot labels (with a Gaussian prior) and calculates the exact value without approximation. The left plot in Figure 6 confirms that both approaches can reflect the trend of feature quality. However, we notice that Laplace approximation has larger fluctuations than LogME, and the Laplace approximation requires more computation than LogME. In addition, its performance in realistic data (Section 6.2.1) is not satisfying. Therefore, when dealing with classification data, we convert classification labels to one-hot labels and treat the problem as a multivariate regression problem in LogME. How to analytically calculate the value with a categorical prior is left as a future research question.

6.2 Ranking pre-trained models

This section focuses on the first part of the proposed paradigm: ranking pre-trained models. The goal is to rank pre-trained models so that potentially best PTMs can be selected for the subsequent tuning process. This section attaches great importance to the diversity of pre-trained models and downstream tasks. Section 6.2.1 and Section 6.2.2 transfer supervised pre-trained models to classification and regression tasks, respectively; Section 6.2.3 explores unsupervised pre-trained models on both classification and regression; Section 6.2.4 and Section 6.2.5 study pre-trained language models on language understanding tasks and a sequential tagging task, respectively. These extensive experiments demonstrate the generality and effectiveness of the proposed LogME in ranking pre-trained models.

6.2.1 RANKING SUPERVISED PRE-TRAINED MODELS IN CLASSIFICATION TASKS

We use 12 ImageNet pre-trained models available from PyTorch: Inception V1 (Szegedy et al., 2015), Inception V3 (Szegedy et al., 2016), ResNet 34 (He et al., 2016), ResNet 50 (He et al., 2016), ResNet 101 (He et al., 2016), ResNet 152 (He et al., 2016), Wide ResNet 50 (Zagoruyko

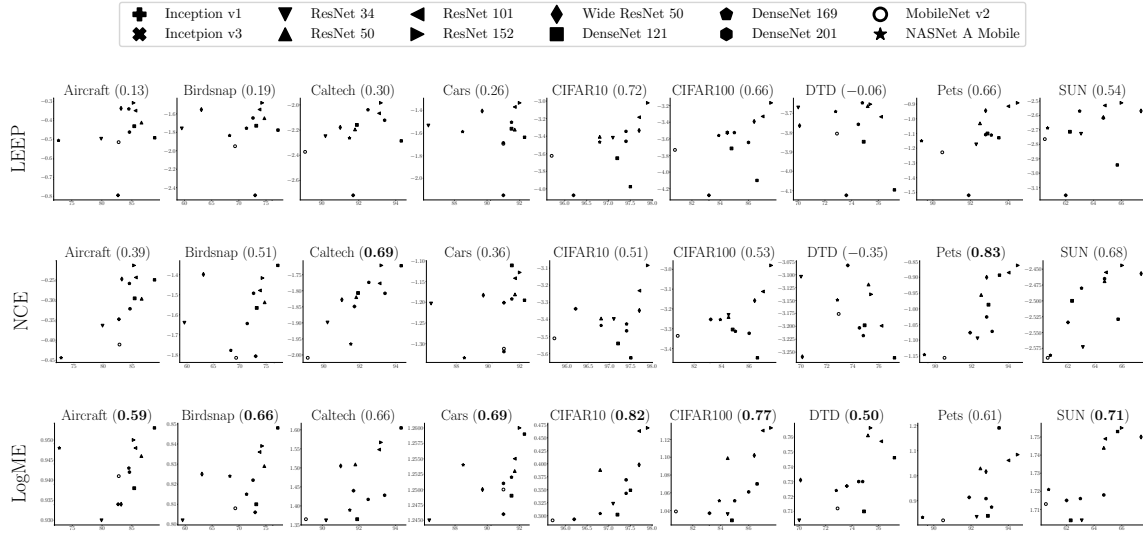


Figure 7: Correlation values (τ_w) between fine-tuned accuracy (X-axis) and scores produced by three methods (Y-axis) for ranking PTMs on 9 datasets with 12 pre-trained models. One row for each method, one column for each dataset (with τ_w in the parenthesis near the dataset name), and one marker for each pre-trained model. The best τ_w in each dataset is marked in bold.

and Komodakis, 2016), DenseNet 121 (Huang et al., 2017), DenseNet 169 (Huang et al., 2017), DenseNet 201 (Huang et al., 2017), MobileNet V2 (Sandler et al., 2018), and NASNet-A Mobile (Tan et al., 2019). These pre-trained models cover most of the supervised pre-trained models in transfer learning that practitioners frequently use.

For downstream classification tasks, we take 9 commonly used datasets: Aircraft (Maji et al., 2013), Birdsnap (Berg et al., 2014), Caltech (Fei-Fei et al., 2004), Cars (Krause et al., 2013), CIFAR10 (Krizhevsky and Hinton, 2009), CIFAR100 (Krizhevsky and Hinton, 2009), DTD (Cimpoi et al., 2014), Pets (Parkhi et al., 2012), and SUN (Xiao et al., 2010). The description of each dataset and data statistics are listed in Appendix F.

For all the datasets we use, we respect the official train/val/test splits if they exist, otherwise we use 60% data for training, 20% data for validation (searching hyper-parameters to measure the reference transfer learning performance) and 20% data for testing. Models are trained with a fixed number of epochs, and the best model in the validation split is used as the final model to be tested in the test split.

To compute the reference transfer learning performance $\{T_m\}_{m=1}^M$ ($M = 12$), we carefully fine-tune pre-trained models with grid-search of hyper-parameters. Li et al. (2020) pointed out that learning rate and weight decay are the two most important hyper-parameters. Hence we grid search learning rate and weight decay (7 learning rates from 10^{-1} to 10^{-4} , 7 weight decays from 10^{-6} to 10^{-3} , all logarithmically spaced) to select the best hyper-parameter on the validation split and compute the accuracy on the test split as the reference transfer learning performance. *It is noteworthy that LogME requires neither fine-tuning nor grid search.* Here we fine-tune pre-trained models to see how well do LogME values correlate

with the reference transfer performance, but practitioners can straightforwardly use LogME to evaluate pre-trained models without fine-tuning.

We compare LogME against LEEP (Nguyen et al., 2020) and NCE (Tran et al., 2019). Results of calculating the evidence using Laplace approximation (Immer et al., 2021) are not shown but listed in the appendix, because its performance is unsatisfying. Before this paper, LEEP and NCE were the only two methods to rank PTMs without fine-tuning, and they can only rank supervised pre-trained models in classification tasks. We use LEEP, NCE, and LogME to compute scores $\{S_m\}_{m=1}^M$ by applying 12 pre-trained models to the datasets. The correlation values τ_w between scores and fine-tuned accuracies are presented in Figure 7.

We can find that LogME has consistently better correlation than LEEP, and outperforms NCE on most datasets (7 datasets out of 9 datasets). Note that LEEP and NCE even show negative correlation values in DTD (Cimpoi et al., 2014), because they rely on the relationship between classes of the pre-trained task and the target task but DTD classes (textures) are very different from ImageNet categories (objects). In contrast, LogME still performs reasonably well for DTD.

According to the interpretation of τ_w in Section 3.1, correlation value τ_w can be roughly translated into $\frac{\tau_w+1}{2}$ probability of correct comparison (concordant pairs). The smallest τ_w of LogME in Figure 7 is around 0.5, so the probability of a pre-trained model ϕ_A transferring better than ϕ_B is about 75% if ϕ_A has a larger LogME. For most tasks τ_w of LogME is 0.7 or 0.8, so the probability of correct selection is 85% or 90%, sufficient for practical usage.

6.2.2 RANKING SUPERVISED PRE-TRAINED MODELS IN A REGRESSION TASK

Besides extensive classification tasks considered above, this section shows how LogME can assess pre-trained models for a regression task. The two prior methods (LEEP and NCE) depend on the category relationship between pre-trained categories and downstream categories, therefore they do not apply to regression tasks.

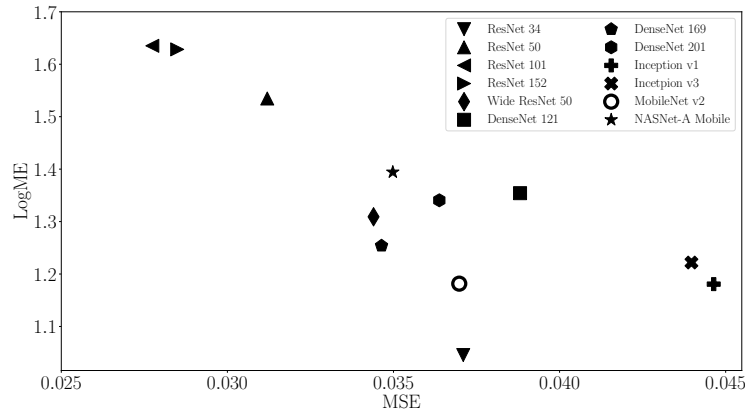


Figure 8: Supervised pre-trained models transferred to dSprites.

The regression task we use is the dSprites (Matthey et al., 2017) dataset from the Visual Task Adaptation Benchmark (Zhai et al., 2020), a common benchmark for evaluating the quality of learned representations. The input is an image containing a sprite (heart, square, and ellipse) with varying scale/orientation/position. Pre-trained models are transferred

to predict four scalars (scale, orientation, and (x, y) positions) together, and mean square error (MSE) on the test data is reported. The supervised pre-trained models and the hyper-parameter tuning scheme are the same as in Section 6.2.1.

Results are plotted in Figure 8. It is clear that LogME and MSE are well correlated and the correlation coefficient $\tau_w = 0.79$ is very large: if a pre-trained model ϕ_A has larger LogME than ϕ_B , with roughly 89.5% probability ϕ_A is better (has smaller MSE) than ϕ_B after actually fine-tuning.

6.2.3 RANKING CONTRASTIVE PRE-TRAINED MODELS IN DOWNSTREAM TASKS

The recently emerged unsupervised pre-trained models (He et al., 2020) have attracted much attention due to their potential ability to exploit humongous unlabeled data on the Internet. They use the contrastive loss (Gutmann and Hyvärinen, 2010) to inject supervision signals into pre-training with unlabeled data, and they feature a projection head with continuous output. Ranking contrastive pre-trained models is an emerging demand, but LEEP and NCE cannot be extended to deal with the projection head of contrastive-based unsupervised pre-trained models because they rely on discrete category relationship.

Since LogME only requires features extracted from pre-trained models, it can be applied to contrastive pre-trained models. To demonstrate this, we use four popular models pre-trained with various training schemes: MoCo V1 (He et al., 2020) with momentum contrast, MoCo V2 (Chen et al., 2020b) with an MLP projection head and strong data augmentation, MoCo 800 trained with 800 epochs as suggested by Chen et al. (2020a), and SimCLR (Chen et al., 2020a) trained by a carefully designed training scheme (Chen et al., 2020a).

For classification, we use Aircraft (Maji et al., 2013), the first dataset (alphabetically) in Section 6.2.1; for regression, we use dSprites (Matthey et al., 2017), the only regression task in this paper. Results are shown in Table 3. SimCLR on dSprites is not reported as it does not converge after several trials, possibly because it is heavily tailored to classification tasks. LogME gives the *perfect order* of both accuracy and MSE. Note that the reference order on transfer learning performance in Aircraft (MoCo V1 < MoCo V2 < MoCo 800) is different from the order in dSprites (MoCo V1 < MoCo 800 < MoCo V2), emphasizing that ranking pre-trained models is *task adaptive*. We also observe that LogME values of unsupervised pre-trained models are similar (the difference is smaller than their supervised counterparts in Section 6.2.1), mainly because unsupervised features are not very discriminative.

Table 3: Use LogME to rank unsupervised pre-trained models.

PTM	Aircraft		dSprites	
	Accuracy (%)	LogME	MSE	LogME
MoCo V1	81.68	0.934	0.069	1.52
MoCo V2	84.16	0.941	0.047	1.64
MoCo 800	86.99	0.946	0.050	1.58
SimCLR	88.10	0.950	-	-
	$\tau_w: 1.0$		$\tau_w: 1.0$	

6.2.4 RANKING PRE-TRAINED LANGUAGE MODELS IN THE GLUE BENCHMARK

To further demonstrate the generality of LogME, we show how LogME can work for pre-trained language models. Again, existing methods (LEEP and NCE) cannot deal with these pre-trained language models.

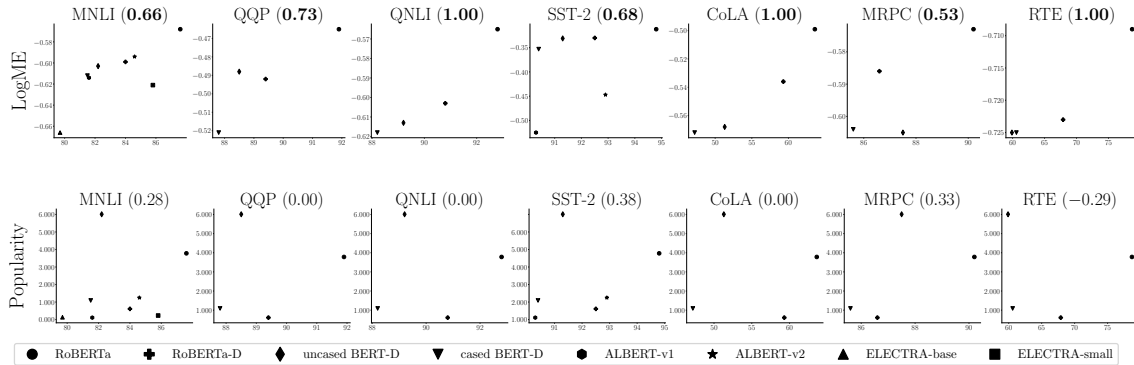


Figure 9: Correlation values (τ_w) between fine-tuned accuracy (X-axis) and LogME value / Popularity value (Y-axis) in 7 GLUE tasks with 8 popular PTMs. One sub-figure for each task (with its τ_w in the parenthesis), and one marker for each PTM.

Here we take another approach to evaluating the reference transfer performance $\{T_m\}_{m=1}^M$. We do not fine-tune pre-trained models, but directly take fine-tuned results from HuggingFace Models, and check if LogME values can correlate well with the results. Specifically, we take pre-trained models that have GLUE performance tuned by the HuggingFace organization, and select the top 8 downloaded models: RoBERTa (Liu et al., 2019), RoBERTa-D, uncased BERT-D, cased BERT-D, ALBERT-v1 (Lan et al., 2020), ALBERT-v2 (Lan et al., 2020), ELECTRA-base (Clark et al., 2020), and ELECTRA-small (Clark et al., 2020) (“D” means distilled version). The LogME values on 7 GLUE tasks together with fine-tuned accuracies are plotted in Figure 9. Some models only have results for certain tasks and we keep them as they are. Even though these accuracy numbers are tuned by the HuggingFace organization, LogME perfectly estimates the ranking of transfer performance for 3 tasks (with $\tau_w = 1$), showing the surprising effectiveness of LogME in ranking pre-trained models.

One may wonder how well does a pre-trained model’s popularity indicate its transfer learning performance, because it is a common belief that PTMs with consistent improvements across many tasks may tend to become popular. To answer this question, a quantitative measurement of popularity is required. Two possible quantities are considered: the citation number of the paper proposing the pre-trained model, and the download count of the pre-trained model. The paper citation number is not a proper metric for assessing individual PTM’s transferability, because one paper can contain many PTMs. For example, the BERT paper (Devlin et al., 2019) contains BERT-base and BERT-large, they have the same citation number but are in different transferability levels. Download count is a PTM-wise well-defined metric, hence we can use it as a proxy for popularity.

Thanks to the public data from HuggingFace, each PTM’s download count (measured in millions) is available to approximate the popularity. The bottom figure in Figure 9 shows how well popularity performs when it is used as a transferability metric. It is clear that popularity

does not correlate well with transfer learning performance: *the τ_w values of popularity are significantly lower than LogME’s τ_w values*, and negative correlation value occurs in the RTE task. Note that BERT models are the most popular but RoBERTa is the best among these tasks, revealing a mismatch between popularity and transfer learning performance. The above experiments again echo with the motivation of this paper: practitioners usually select the most popular pre-trained model due to the lack of a satisfying selection strategy, and LogME can come to their rescue.

6.2.5 RANKING PRE-TRAINED LANGUAGE MODELS IN A SEQUENTIAL TAGGING TASK

So far, we have only considered simple classification and regression tasks. It would be valuable to extend LogME to tasks with structured output such as object detection and semantic segmentation. Next we show how LogME can be used in a sequential tagging task where both the input and the output are structured. How to deal with a general task with structured output is left as future work.

The specific task we consider in this section is named entity recognition (Sang and De Meulder, 2003). It requires the model to predict the entity label (person, location, organization, etc.) of every token in a sentence, therefore the output is structured. Considering that the named entity recognition task is sometimes referred to as “token-level classification”, we can flatten the token dimension to apply LogME. The only change is that n represents the number of tokens rather than the number of sentences.

We use the same PTMs as in Section 6.2.4, and the dataset is CoNLL-2003 (Sang and De Meulder, 2003) whose performance is measured by F-1 score. Table 4 holds the results. The rank correlation value τ_w is 0.20, smaller than results in previous sections. The small τ_w is caused by an outlier PTM named RoBERTa (Liu et al., 2019), which has the largest F-1 score with a relatively small LogME value. We conjecture that RoBERTa has a small LogME value because it is trained much longer than BERT in the masked language modeling task, which might make its representation tailored to the task, lowering its LogME score in the dissimilar task of named entity recognition. On the other hand, RoBERTa is robustly optimized, so it can be easily fine-tuned to downstream tasks with competitive results.

If we select the best PTM by the largest LogME value, ALBERT-v1 will be used and its performance is comparable to the best (97.0% *vs.* 97.4%). From this perspective, LogME is decently useful. In general, how to deal with structured tasks better would be a research problem requiring further efforts.

Table 4: Ranking pre-trained models in named entity recognition (CoNLL-2003 task).

PTM	RoBERTa	RoBERTa-D	uncased BERT-D	cased BERT-D	ALBERT-v1	ALBERT-v2	ELECTRA-base	ELECTRA-small	τ_w
F-1 score (%)	97.4	96.6	96.8	95.5	97.0	97.4	97.2	91.9	
LogME	0.685	0.723	0.783	0.623	0.834	0.809	0.746	0.646	0.20

6.3 Tuning pre-trained models

This section turns to the second part of the proposed paradigm: tuning pre-trained models. As mentioned in Section 5, most academic researchers are not constrained by the inference cost of deployed models, and they can use the best-ranked (according to the LogME value)

PTM straightforward. This paper is concerned about the practical usage scenario, where computational constraints require us to use a specific PTM but we still want to leverage the knowledge from other PTMs in the pre-trained model hub.

Experiments in this section are designed to compare three methods of tuning multiple PTMs: the knowledge distillation approach, the Zoo-tuning approach and the proposed B-Tuning. We first conduct experiments with multiple homogeneous PTMs where all three methods are applicable, then we dive into the practical case of multiple heterogeneous PTMs. By default, the temperature scaling hyper-parameter t is set to 0.1 in Equation 5.

6.3.1 TUNING MULTIPLE HOMOGENEOUS PTMs

We use five homogeneous pre-trained models following the experimental setup of Zoo-tuning (Shu et al., 2021). They are ResNet-50 models trained by different pre-training tasks: (1) Supervised pre-trained on ImageNet (He et al., 2016); (2) Unsupervised pre-trained by MoCo (He et al., 2020); (3) MaskRCNN model (He et al., 2017); (4) DeepLab V3 (Chen et al., 2017); (5) KeyPoint detection model pre-trained on COCO (Lin et al., 2014). The dataset we use is Aircraft (Maji et al., 2013), the first dataset (alphabetically) in Section 6.2.1. The target model is ResNet-50 pre-trained in ImageNet, following the setting of Shu et al. (2021).

To demonstrate the effectiveness of B-Tuning, we use all five PTMs as the teacher models, and report the performance of three methods (B-Tuning, knowledge distillation, and Zoo-tuning) on multiple PTM tuning in the first row of Table 5. Zoo-tuning performs better than vanilla knowledge distillation, and the proposed B-Tuning even surpasses Zoo-tuning, setting a new state-of-the-art result for multiple PTMs tuning.

Table 5: Accuracy (%) of multiple PTMs tuning in Aircraft, with different teacher models and tuning methods. As a baseline, single PTM fine-tuning yields 82.99% accuracy.

method teacher models	Knowledge Distillation	Zoo-tuning	B-Tuning
all PTMs from the PTM hub	82.97 ± 0.27	83.32 ± 0.32	83.49 ± 0.17
top-3 PTMs (ranked by LogME)	84.29 ± 0.30	-	85.12 ± 0.15

To demonstrate the effectiveness of LogME selection in multiple PTM tuning, we rank five PTMs by LogME, and select the top- K PTMs as the teacher models in the subsequent tuning. Shu et al. (2021) used all five PTMs to tune the target PTM, since they do not investigate how to select PTMs. To sufficiently test the effect of selection, we choose $K = \arg \max_{3 \leq K \leq 5} \binom{5}{K} = 3$, so that there are many possible selections and later we can explore how optimal LogME selection is. The results are in the second row of Table 5. Surprisingly, selecting top-3 PTMs brings a significant performance improvement, demonstrating the effectiveness of the “ranking and tuning pre-trained models” paradigm.

To evaluate the optimality of LogME selection, we try all the $\binom{5}{3} = 10$ combinations of selecting 3 PTMs from 5 PTMs. Vanilla knowledge distillation is used to avoid confounders. Results are shown in Figure 10, with the accuracy of fine-tuning a single ResNet-50 as the baseline. We have two observations from Figure 10: (1) Transferring the knowledge from multiple PTMs consistently outperforms fine-tuning a single pre-trained model (82.99%), which adheres to our intuition that utilizing the rich knowledge from various PTMs is better

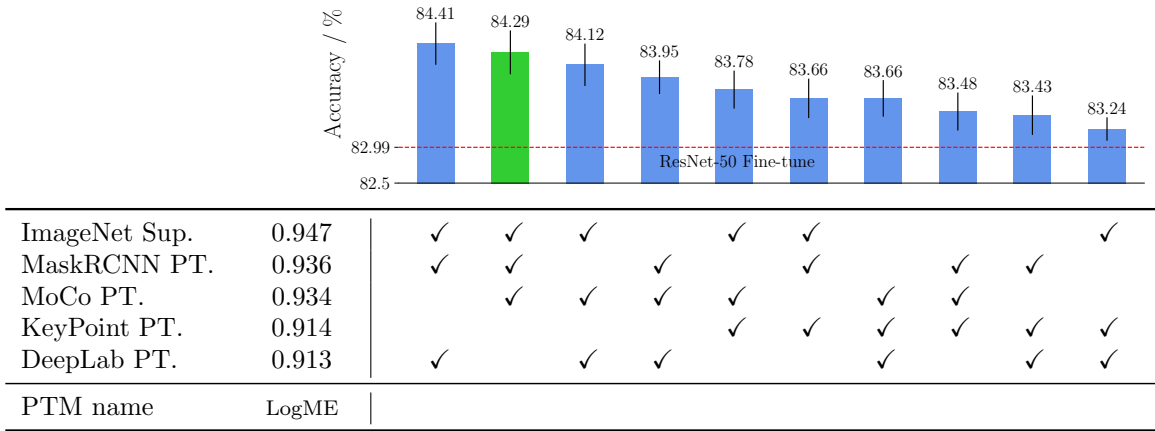


Figure 10: Accuracy of knowledge distillation with 3 PTM teachers. All $\binom{5}{3} = 10$ combinations of selecting 3 PTM teachers are reported. Selecting top-3 PTMs according to LogME achieves the second best performance among 10 combinations.

than fine-tuning alone. (2) The best combination achieves 84.41% accuracy, but usually it is too expensive to try all the combinations (10 trials). Instead, we can use LogME to select the top-3 PTMs, which achieves 84.29% accuracy and is the second best. Moreover, we can select the top-3 PTMs by LogME and then perform B-Tuning, which even surpasses the best combination and has an accuracy of 85.12%.

We can draw three conclusions from experiments in this section: (1) multiple PTMs tuning is better than single PTM fine-tuning; (2) it is better (near-optimal among all the possible selections) to select top-ranked PTMs according to LogME than to use all the PTMs; (3) B-Tuning is superior to knowledge distillation and Zoo-tuning.

In addition, we would like to point out that selection based on LogME value is a greedy procedure, which could fail to capture the complicated high-order interaction among PTMs. For example, in Figure 10, DeepLab pre-trained model has the lowest LogME value, but it appears in the best combination. How to analyze the high-order interaction among PTMs would be a worthwhile research question in the future. The goal of this section is to show the greedy selection based on LogME value has a reasonably good performance.

6.3.2 TUNING MULTIPLE HETEROGENEOUS PTMs

Section 6.3.1 studies multiple PTMs tuning with homogeneous models, which follows the setting of Shu et al. (2021) and demonstrates the superiority of B-Tuning. Nonetheless, compared with tuning multiple homogeneous PTMs, a more general and more attractive application of multiple PTMs tuning is to transfer knowledge from a large hub of heterogeneous PTMs. This section focuses on the latter setting, and provides some guidelines on how to select a proper number of PTMs (*i.e.*, the hyper-parameter K) as teachers.

The alphabetically first and second datasets (Aircraft and Birdsnap) are chosen and the PTM hub consists of the 12 PTMs used in Section 6.2.1. The 12 PTMs are ranked by their

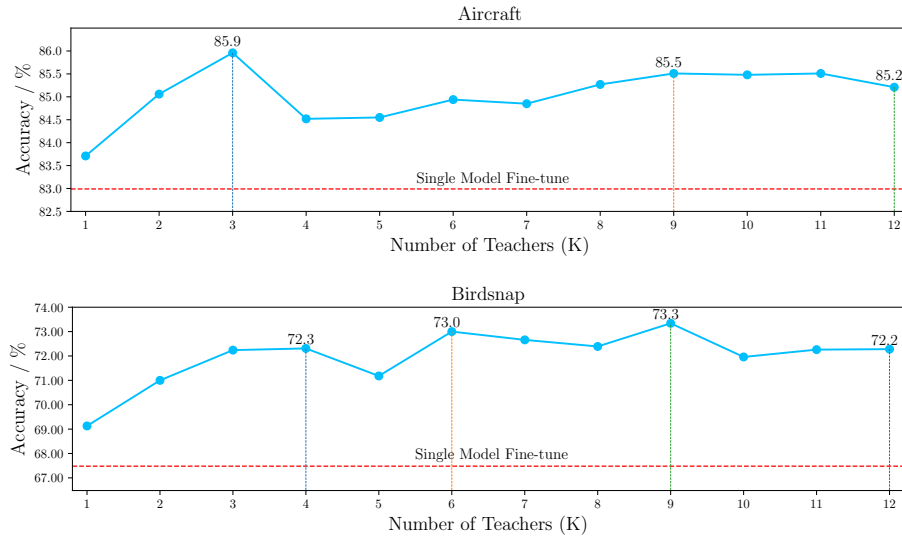


Figure 11: A study on the number of PTMs (K) to use in B-Tuning with two datasets (Top: Aircraft; Bottom: Birdsnap).

LogME values, and the target PTM ϕ_t is the most common ResNet-50. Top- K PTMs are used in B-Tuning to fine-tune the target model, with K varying from 1 to 12. Results are plotted in Figure 11, where the X-axis is the value of K .

We conclude the following observations from Figure 11: (1) B-Tuning with multiple PTMs is consistently better than single PTM fine-tuning. (2) B-Tuning with all the 12 PTMs does not yield the best accuracy, which emphasizes the importance of selecting proper PTMs. (3) The trend of accuracy with respect to K is complicated, and how to select an optimal K can be a valuable topic for future researchers.

For practitioners, there are two concerns about the choice of K : (1) choosing the optimal K can yield the best accuracy; (2) but larger K incurs a much larger computational cost, since a forward pass of each PTM during tuning is required. Considering the results in Figure 11 and the trade-off between the computational cost and the performance improvement, we recommend choosing K from 2, 3, and 4 in practice.

6.4 Using ImageNet-1K as the downstream task

The above experiments focus on small-scale and medium-scale downstream tasks, which are common in transfer learning research. This section takes a step further to use the large-scale ImageNet-1K (Deng et al., 2009) as the downstream dataset. In this case, a dataset larger than ImageNet-1K should be used for pre-training. JFT-300M (Sun et al., 2017), Instagram-1B (Mahajan et al., 2018), and ImageNet-21K (Deng et al., 2009) are commonly-used datasets that are larger than ImageNet-1K. Among them, ImageNet-21K is the only publicly available dataset, which serves as the pre-training dataset here. ImageNet-21K pre-trained models are provided by the timm project. It mainly contains models pre-trained on ImageNet-1K, but also has three models pre-trained on ImageNet-21K and fine-tuned

on ImageNet-1K, including MLP-Mixer (Tolstikhin et al., 2021), ViT (Dosovitskiy et al., 2021), and Swin-T (Liu et al., 2021b). With ImageNet-1K as the downstream dataset, their LogME score and fine-tuned reference transfer learning performance are presented in Table 6. LogME is perfectly aligned with the reference performance, with a correlation value $\tau_w = 1$. Then we use B-Tuning to tune the commonly used ResNet-50 trained in ImageNet-1K, with Vit and Swin as teacher models. The accuracy is increased from 76.15% to 76.50%.

Experiments in this section demonstrate that LogME and B-Tuning work for not only small-scale and medium-scale datasets but also large-scale datasets.

Table 6: Ranking models pre-trained on ImageNet-21K transferred to ImageNet-1K.

PTM pre-trained on ImageNet-21K	MLP-Mixer	ViT	Swin-T	τ_w
Fine-tuned Accuracy on ImageNet-1K (%)	76.61	84.53	85.25	1.00
LogME value	2.075	2.085	2.134	

6.5 Efficiency of LogME

A theoretically sound algorithm is usually complicated and computationally expensive, as is the case for LogME without optimization. Fortunately, we successfully reduced the computational complexity after analyzing its theoretical convergence property in Section 4.1 by the fixed point iteration. The algorithmic complexity has been analyzed in Table 2, and Table 7 presents the wall-clock time speedup measured in Aircraft with ResNet-50. The naïve implementation is very slow. Our conference paper (You et al., 2021) proposed an optimization scheme for matrix multiplication and matrix inversion, which brings $61.7\times$ speedup. This paper further proposes the fixed point iteration algorithm, which results in a much larger speedup ($131.5\times$). Thanks to the optimized method, LogME is not only theoretically sound but also computationally efficient.

Table 7: Quantitative measurement of computational speedup in evidence maximization.

	Wall-clock time (second)	Speedup
evidence maximization (naïve implementation)	802.5 ± 5.6	-
evidence maximization (optimized by You et al. (2021))	13.1 ± 0.7	$61.7\times$
evidence maximization (fixed point iteration, proposed)	6.1 ± 0.7	$131.5\times$

Next, we quantitatively measure the wall-clock and memory footprint of LogME in both computer vision and natural language processing in Table 8. ResNet 50 on Aircraft is used for computer vision, and RoBERTa-D on MNLI task is used for NLP. The cost for the rest of the models and datasets varies, but the proportion is similar. The cost of computing reference transferability T_m (fine-tuning with hyper-parameter search) serves as the upper bound of ranking pre-trained models. Note that, because carelessly tuned hyper-parameters cannot tell good models apart from bad models, it is necessary to attribute the cost of hyper-parameter search to fine-tuning. We also list the cost of extracting features by pre-trained models, which is the lower bound of ranking pre-trained models.

Table 8: Computational cost and memory footprint of LogME.

	wall-clock time	memory footprint
Computer Vision	fine-tune (upper bound) 161000s	fine-tune (upper bound) 6.3 GB
	extract feature (lower bound) 37s	extract feature (lower bound) 43 MB
	LogME 43s	LogME 53 MB
	benefit 3700 \uparrow	benefit 120 \uparrow
Natural Language Processing	fine-tune (upper bound) 100200s	fine-tune (upper bound) 88 GB
	extract feature (lower bound) 1130s	extract feature (lower bound) 1.2 GB
	LogME 1136s	LogME 1.2 GB
	benefit 88 \uparrow	benefit 73 \uparrow

According to Table 8, we have the following observations: (1) brute-force fine-tuning is computationally expensive, requiring about a day for one dataset with one pre-trained model. Selecting the best pre-trained model out of 12 models would cost 12 GPU-days. (2) Extracting features is very cheap and costs much less than fine-tuning. (3) The additional time-cost of LogME compared to feature extraction is rather small, which means that *LogME’s cost is very close to the lower bound*. In computer vision, LogME is $3700\times$ faster than fine-tuning, with $120\times$ less memory footprint. In the NLP domain, feature extraction is much slower than that in computer vision, and therefore the wall-clock time speedup ($73\times$) is not that striking.

In summary, LogME is efficient in terms of both wall-clock time and memory footprint, thanks to the optimized algorithm (fixed point iteration) inspired by the theoretical analysis.

6.6 Comparing LogME to re-training head

A straightforward way to measure the relationship between features and labels is to train a linear classification/regression head for the downstream task, and to use the head’s performance as a metric, which is known as “*linear probing*” or “*linear protocol evaluation*”. Empirically, we find that re-training head does not work well. In the following, we summarize why re-training head is inferior to LogME from three perspectives, which partially explains why the important problem of ranking and tuning PTMs was under-explored in the past.

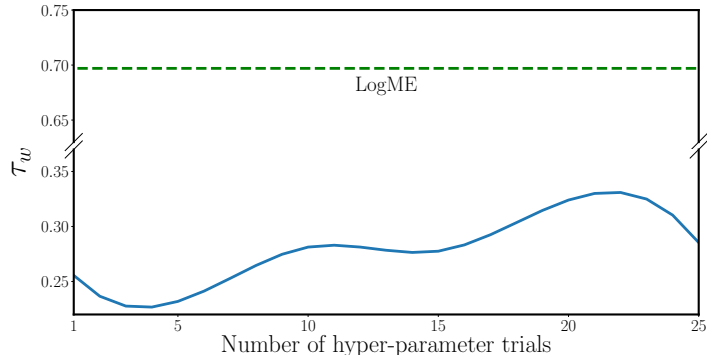


Figure 12: The correlation of re-training head w.r.t. the number of hyper-parameter trials.

(1) LogME is more efficient than re-training head. In linear protocol evaluation, parameters in the head are learned by maximum likelihood estimation, which is prone to over-fitting. To alleviate over-fitting, grid search for its hyper-parameters (such as the strength of L2 regularization) should be tuned extensively on a validation set, making head re-training inefficient. For example, in the Caltech dataset, we extract features from 12 PTMs, train softmax regressors with tuned hyper-parameters (the L2 regularization strength), and plot the correlation τ_w between the best head accuracy and the reference transfer performance w.r.t. the number of hyper-parameter trials in Figure 12. The correlation of LogME is plotted as a reference. Computing LogME requires $3 \times$ less time than re-training a head with one fixed hyper-parameter, and re-training head with exhaustive hyper-parameter search is still much inferior to LogME.

(2) Re-training head does not work well with limited training data. Because re-training head follows a supervised learning paradigm, it suffers in low-shot learning scenarios. For example, prompt learning (Liu et al., 2021a) is an active research area in natural language processing, where researchers try to exploit the potential of frozen pre-trained models by only a few training data. In the sentiment classification task SST-2 (Socher et al., 2013), prompt learning (Liu et al., 2021a) extracts the sentence embedding E_S for each sentence S , and compare E_S with word embeddings E_P, E_N of a positive anchor word P (such as “good” and “fantastic”) and a negative anchor word N (such as “bad” and “awful”). The decision rule is: **sentence S contains positive sentiment $\iff E_S^T E_P > E_S^T E_N$** . In this case, searching proper anchor words on validation data yields 61.4% accuracy (complete results are available in Table 13). Re-training head (*i.e.*, training a simple classification head with limited training data on frozen sentence embedding E_S and tuning the weight-decay hyper-parameter on validation set) only achieves 51.64% accuracy with 10 sentences for training. Meanwhile, we can apply LogME (or to be specific, the posterior predictive distribution introduced in Section 5.3) to this problem, which does not require any hyper-parameter tuning. This way, we can combine training data with validation data to compute the predictive weight m for each class, and use m as the embedding of a virtual “anchor word”, which results in 79.24% accuracy, *a huge improvement over re-training head and manually selected anchor words!* The superior performance of LogME is interpretable: we analyzed the predictive weight m for the negative sentiment class, and find that it is closest to the embedding of “dump”, “:(”, “doomed”, “worse”, “worse”. To our surprise, it can discover that “:(”, a cyber word to express unhappy emotion, contains negative sentiment.

(3) Re-training head does not have a clear metric. As a side issue, even if we re-train a head for a downstream task, it is unclear which quantity should be used as the ranking metric. When the performance of a downstream task is evaluated by accuracy or MSE, is it over-fitting to use the accuracy or MSE of the re-trained head? Indeed, in Figure 12, when the number of hyper-parameter trials increases, the correlation can even go down, confirming the concern of over-fitting. In contrast, LogME has unified modeling of label evidence, which has a clear statistical support.

7. Conclusion

Pre-trained models are universally acknowledged as the foundation of deep learning. Researchers have explored a lot how to create and exploit PTMs. In this paper, we switch from individual PTMs to PTM hubs, and study how to sufficiently exploit PTM hubs with a new paradigm of ranking and tuning pre-trained models. The ranking part introduces a theoretically sound and computationally efficient transferability metric named LogME. The theoretical investigation of LogME solved the decades-long unanswered question about the convergence of the MacKay’s algorithm. LogME is then further extended to be a multiple PTMs tuning method named B-Tuning, which completes the tuning part of the paradigm.

The extensive experiments confirm the effectiveness of the proposed methods in ranking (LogME *vs.* brute-force fine-tuning/LEEP/NCE), selection (top- K PTMs by LogME *vs.* exponentially many combinations), and tuning (B-Tuning *vs.* Zoo-tuning and Knowledge Distillation), making the new paradigm of exploiting PTM hubs attractive for practitioners.

Acknowledgments

We would like to dedicate our thanks to Ximei Wang, Xinyang Chen, Yang Shu at Tsinghua University, Yi Zeng at Peking University, and Yonglong Tian at MIT for helpful discussions. Kaichao You, Yong Liu, Jianmin Wang, and Mingsheng Long are supported by the National Megaproject for New Generation AI (2020AAA0109201), the National Natural Science Foundation of China (62022050 and 62021002), the Beijing Nova Program (Z201100006820041), the BNRist Scholar Fund (BNR2021RC01002), and the Tsinghua-Huawei Innovation Fund.

A. Notation Table

Notations used in this paper are listed in the following table. We tried our best to avoid notation conflicts, but the following notation conflicts are unavoidable due to the heavy math in this paper: (1) f_i represents features of x_i and $f(t)$ represents the fixed point iteration function. (2) w represents parameters in the linear head while the weighted Kendall's rank correlation τ_w uses w as its subscript. (3) t is used in the convergence proof and also used for the temperature hyper-parameter in B-Tuning.

Table 9: Notations used in this paper.

notation	dimensionality	meaning
i, j, k	\mathbb{N}	running subscripts
M, n	\mathbb{N}	the number of PTMs and samples
K	\mathbb{N}	the number of selected PTMs for subsequent tuning
C, D	\mathbb{N}	the dimension of label and extracted feature
ϕ	—	a pre-trained model
x_i	—	an input sample
$f_i = \phi(x_i)$	\mathbb{R}^D	extracted feature of an input example
$F = [f_1, \dots, f_n]^T$	$\mathbb{R}^{n \times D}$	stacked features of f_i
Y_i	\mathbb{R}^C	label of x_i
y_i	\mathbb{R}	a component of Y_i
y	\mathbb{R}^n	the label component for all n samples
y'	—	predictive distribution of an input sample
$\pi_k = \frac{\exp(\mathcal{L}_k/t)}{\sum_{j=1}^K \exp(\mathcal{L}_j/t)}$	\mathbb{R}	weighted coefficient for each teacher model ϕ_k
$\bar{y}' = \sum_{k=1}^K \pi_k y'_k$	—	weighted average of y'
T	\mathbb{R}	reference transfer performance
S	\mathbb{R}	score produced by a transferability metric
τ	\mathbb{R}	Kendall's rank correlation
τ_w	\mathbb{R}	weighted Kendall's rank correlation
w	\mathbb{R}^D	parameter in linear head
α/β	\mathbb{R}	hyper-parameter of the Bayesian linear model
$A = \alpha I_D + \beta F^T F$	$\mathbb{R}^{D \times D}$	a quantity in calculating LogME
$m = \beta A^{-1} F^T y$	\mathbb{R}^D	a quantity in calculating LogME
γ	\mathbb{R}	a quantity in calculating LogME
$\mathcal{L} = \mathcal{L}(\alpha, \beta)$	\mathbb{R}	log evidence given α, β
α^*, β^*	\mathbb{R}	α, β to achieve maximum evidence
U, Σ, V	—	matrices in SVD ($F = U \Sigma V^T$)
σ	\mathbb{R}	diagonal entries in Σ
r	\mathbb{N}	the rank of matrix F
$z = U^T y$	\mathbb{R}^n	transformation of y under U
$t = \frac{\alpha}{\beta}$	\mathbb{R}	a quantity in convergence proof
t', α', β'	\mathbb{R}	the value of t, α, β after an iteration
$f(t)$	—	the fixed point iteration function
$\tilde{\mathcal{L}}, \tilde{F}$	—	\mathcal{L}, F for duplicated or padded features
W	—	transformation matrix in knowledge distillation

B. Proof of Theorem 1

Theorem 1: Algorithm 4 induces a scalar function $t' = f(t) = \left(\frac{n}{n - \sum_{i=1}^D \frac{\sigma_i^2}{t + \sigma_i^2}} - 1 \right) t^2 \frac{\sum_{i=1}^n \frac{z_i^2}{(t + \sigma_i^2)^2}}{\sum_{i=1}^n \frac{\sigma_i^2 z_i^2}{(t + \sigma_i^2)^2}}$.

Proof Let's express all symbols in a unified form with respect to $\alpha, \beta, \Sigma, z, U, V$:

- $A = \alpha I + \beta F^T F = V(\alpha I + \beta \Sigma^T \Sigma)V^T$
- $A^{-1} = V\Sigma_{inv}V^T$ where $(\Sigma_{inv})_{ii} = \frac{1}{\alpha + \beta \sigma_i^2}$ ($1 \leq i \leq D$)
- $m = \beta A^{-1} F^T y = \beta V\Sigma_{inv}\Sigma^T z$
- $m^T m = z^T \Sigma_m z$ with $\Sigma_m = \beta^2 \Sigma \Sigma_{inv}^2 \Sigma^T$ and $(\Sigma_m)_{ii} = \frac{\beta^2 \sigma_i^2}{(\alpha + \beta \sigma_i^2)^2}$, so $m^T m = \sum_{i=1}^n \frac{\beta^2 \sigma_i^2 z_i^2}{(\alpha + \beta \sigma_i^2)^2}$
- $Fm = \beta U \Sigma \Sigma_{inv} \Sigma^T z$, $Fm - y = U \Sigma_{res} z$ with $\Sigma_{res} = \beta \Sigma \Sigma_{inv} \Sigma^T - I$, $(\Sigma_{res})_{ii} = -\frac{\alpha}{\alpha + \beta \sigma_i^2}$
- $\|Fm - y\|_2^2 = (Fm - y)^T (Fm - y) = z^T (\Sigma_{res})^2 z = \sum_{i=1}^n \frac{\alpha^2 z_i^2}{(\alpha + \beta \sigma_i^2)^2}$
- $\gamma = \sum_{i=1}^D \frac{\beta \sigma_i^2}{\alpha + \beta \sigma_i^2} = \sum_{i=1}^D \frac{\sigma_i^2}{t + \sigma_i^2}$

Putting them together, we have

$$t' = \frac{\alpha'}{\beta'} = \frac{\gamma}{n - \gamma} \frac{\|Fm - y\|_2^2}{m^T m} = \left(\frac{n}{n - \sum_{i=1}^D \frac{\sigma_i^2}{t + \sigma_i^2}} - 1 \right) t^2 \frac{\sum_{i=1}^n \frac{z_i^2}{(t + \sigma_i^2)^2}}{\sum_{i=1}^n \frac{\sigma_i^2 z_i^2}{(t + \sigma_i^2)^2}} = f(t)$$

■

C. Proof of Theorem 2

Theorem 2: If $r < n$ and $\sum_{1 \leq i, j \leq n} (z_i^2 - z_j^2)(\sigma_i^2 - \sigma_j^2) > 0$, then $f(t)$ has a fixed point and thus the MacKay's algorithm will converge.

Proof The theorem can be proved by studying the behavior of $f(t)$ near 0 and ∞ .

We have $\lim_{t \rightarrow 0} f(t) = \frac{r}{n-r} \frac{\sum_{i=r+1}^n z_i^2}{\sum_{i=1}^r z_i^2} > 0$, which is a constant and positive number.

When t approaches infinity, we find that $\lim_{t \rightarrow \infty} \frac{f(t)}{t} = \frac{\sum_{i=1}^n \sigma_i^2}{n} \frac{\sum_{i=1}^n z_i^2}{\sum_{i=1}^n \sigma_i^2 z_i^2}$ is constant, which means $f(t)$ behaves linearly when t is large enough.

Noticing a trick used in proving the Chebyshev's Sum Inequality (Hardy et al., 1952), we can get $\sum_{1 \leq i, j \leq n} (z_i^2 - z_j^2)(\sigma_i^2 - \sigma_j^2) = 2n \sum_{i=1}^n \sigma_i^2 z_i^2 - 2(\sum_{i=1}^n \sigma_i^2)(\sum_{i=1}^n z_i^2)$. The condition $\sum_{1 \leq i, j \leq n} (z_i^2 - z_j^2)(\sigma_i^2 - \sigma_j^2) > 0$ thus translates into $\frac{\sum_{i=1}^n \sigma_i^2}{n} \frac{\sum_{i=1}^n z_i^2}{\sum_{i=1}^n \sigma_i^2 z_i^2} < 1$, which means $f(t)$ increases linearly with a slope smaller than 1 (i.e., $\lim_{t \rightarrow \infty} \frac{f(t)}{t} = \frac{\sum_{i=1}^n \sigma_i^2}{n} \frac{\sum_{i=1}^n z_i^2}{\sum_{i=1}^n \sigma_i^2 z_i^2} < 1$).

In summary, When t approaches 0, it is assured that $\lim_{t \rightarrow 0} f(t) > t = 0$; when t is large enough, it is assured that $f(t) < t$. **Putting these two conditions together, they imply the existence of a fixed point $t_0 > 0$ such that $f(t_0) = t_0$.** ■

D. Proof of Corollary 3

Corollary 3: LogME value will remain the same if the feature consists of arbitrary replicas of the original feature. Formally speaking, if the LogME value for $F \in \mathbb{R}^{n \times D}$ and $y \in \mathbb{R}^n$ is \mathcal{L} , then the LogME value for $\tilde{F} = [F, \dots, F] \in \mathbb{R}^{n \times qD}$ and $y \in \mathbb{R}^n$ is also \mathcal{L} . ($q \in \mathbb{N}$ is a natural number to represent the number of replicas.)

Proof Since LogME is calculated via an iterative algorithm, we prove the corollary by an iterative invariant (a quantitative relation that holds after every while-loop iteration).

Preliminary: SVD of \tilde{F} . We have already known the SVD of F is $F = U\Sigma V^T$, and σ_i is the i -th largest eigenvalue of FF^T . Since $\tilde{F}\tilde{F}^T = qFF^T$, duplicated feature \tilde{F} has singular values $\tilde{\sigma}_i^2 = \begin{cases} q\sigma_i^2 & 1 \leq i \leq D \\ 0 & D+1 \leq i \leq qD \end{cases}$, and its left orthogonal matrix is the same as F : $\tilde{U} = U$. The right orthogonal matrix of \tilde{F} is somewhat complicated. Let's find an orthogonal matrix $Q_{q \times q}$, whose entries in the first column are $\frac{1}{\sqrt{q}}$. Entries in the other columns do not matter, as long as $Q_{q \times q}$ is a valid orthogonal matrix. For example, we can

use $Q_{2 \times 2} = \begin{bmatrix} \frac{1}{\sqrt{2}} & -\frac{1}{\sqrt{2}} \\ \frac{1}{\sqrt{2}} & \frac{1}{\sqrt{2}} \end{bmatrix}$, and $Q_{3 \times 3} = \begin{bmatrix} \frac{1}{\sqrt{3}} & -\frac{1}{\sqrt{6}} & -\frac{1}{\sqrt{2}} \\ \frac{1}{\sqrt{3}} & \frac{2}{\sqrt{6}} & 0 \\ \frac{1}{\sqrt{3}} & -\frac{1}{\sqrt{6}} & \frac{1}{\sqrt{2}} \end{bmatrix}$. Then the right orthogonal

matrix of \tilde{F} is $\tilde{V} = Q_{q \times q} \otimes V$, where \otimes is the Kronecker product of two matrices. Using the

block matrix form of Kronecker product, we can write down \tilde{V} as $\tilde{V} = \begin{bmatrix} \frac{1}{\sqrt{p}}V & \dots & \dots \\ \vdots & \ddots & \vdots \\ \frac{1}{\sqrt{p}}V & \dots & \dots \end{bmatrix} \in R^{qD \times qD}$, with the first D columns of \tilde{V} corresponding to singular values $\sqrt{q}\sigma_i, 1 \leq i \leq D$, and the other $(q-1) \times D$ columns of \tilde{V} are orthogonal basis with respect to singular values $\sigma_i = 0$. In summary, if the SVD of F is $F = U\Sigma V^T$, then the SVD of $\tilde{F} = [F, \dots, F]$ is

$\tilde{F} = \tilde{U}\tilde{\Sigma}\tilde{V}^T$, where $\tilde{U} = U, \tilde{\Sigma} = [\sqrt{q}\Sigma, 0, \dots, 0], \tilde{V} = \begin{bmatrix} \frac{1}{\sqrt{q}}V & \dots & \dots \\ \vdots & \ddots & \vdots \\ \frac{1}{\sqrt{q}}V & \dots & \dots \end{bmatrix} = Q_{q \times q} \otimes V$.

Iterative invariant: if we apply Algorithm 2 to both \tilde{F} and F , with a small change that we initialize $\tilde{\alpha} = q, \tilde{\beta} = 1$, then $\tilde{\alpha} = q\alpha, \tilde{\beta} = \beta$ holds before Line 5. Suppose $\tilde{\alpha} = q\alpha, \tilde{\beta} = \beta$ holds before a while-loop, then we can have:

$$\begin{aligned} \tilde{\gamma} &= \sum_{i=1}^{qD} \frac{\tilde{\beta}\tilde{\sigma}_i^2}{\tilde{\alpha} + \tilde{\beta}\tilde{\sigma}_i^2} = \sum_{i=1}^D \frac{q\beta\sigma_i^2}{q\alpha + q\beta\sigma_i^2} = \sum_{i=1}^D \frac{\beta\sigma_i^2}{\alpha + \beta\sigma_i^2} = \gamma \\ \tilde{\Lambda} &= \text{diag} \left\{ \tilde{\alpha} + \tilde{\beta}\tilde{\sigma}_i^2 \right\}, \tilde{\alpha} + \tilde{\beta}\tilde{\sigma}_i^2 = \begin{cases} q(\alpha + \beta\sigma_i^2) & 1 \leq i \leq D \\ q\alpha & D+1 \leq i \leq qD \end{cases} \end{aligned}$$

$$\begin{aligned}
 \tilde{m} &= \tilde{\beta} \tilde{A}^{-1} \tilde{F}^T y = \beta \tilde{V} \tilde{\Lambda}^{-1} \tilde{V}^T \tilde{V} \tilde{\Sigma}^T \tilde{U}^T y = \beta \tilde{V} \tilde{\Lambda}^{-1} \tilde{\Sigma}^T U^T y \\
 &= \beta \left(\begin{bmatrix} \frac{1}{\sqrt{q}} V & \dots & \dots \\ \vdots & \ddots & \vdots \\ \frac{1}{\sqrt{q}} V & \dots & \dots \end{bmatrix} \begin{bmatrix} \frac{1}{q} \Lambda^{-1} & \\ & \frac{1}{q\alpha} I_{(q-1) \times D} \end{bmatrix} \begin{bmatrix} \sqrt{q} \Sigma^T \\ 0 \\ \dots \\ 0 \end{bmatrix} \right) U^T y \\
 &= \begin{bmatrix} \frac{1}{q} V \Lambda^{-1} U^T y \\ \dots \\ \frac{1}{q} V \Lambda^{-1} U^T y \end{bmatrix} = \begin{bmatrix} \frac{1}{q} m \\ \dots \\ \frac{1}{q} m \end{bmatrix}
 \end{aligned}$$

$$\text{Therefore } \tilde{m}^T \tilde{m} = \frac{1}{q} m^T m, \tilde{F} \tilde{m} = [F, \dots, F] \begin{bmatrix} \frac{1}{q} m \\ \dots \\ \frac{1}{q} m \end{bmatrix} = F m.$$

$$\text{After the while-loop iteration, } \tilde{\alpha}' = \frac{\tilde{\gamma}}{\tilde{m}^T \tilde{m}} = \frac{\gamma}{\frac{1}{q} m^T m} = q\alpha', \tilde{\beta}' = \frac{n-\tilde{\gamma}}{\|\tilde{F} \tilde{m} - y\|_2^2} = \frac{n-\gamma}{\|F m - y\|_2^2} = \beta',$$

then the iterative invariant $\tilde{\alpha} = q\alpha, \tilde{\beta} = \beta$ still holds. Therefore we know that when the algorithm converges, $\tilde{\alpha}^* = q\alpha^*, \tilde{\beta}^* = \beta^*$. The corresponding maximum evidence is

$$\begin{aligned}
 \tilde{\mathcal{L}} &= \frac{n}{2} \log \tilde{\beta}^* + \frac{qD}{2} \log \tilde{\alpha}^* - \frac{n}{2} \log 2\pi - \frac{\tilde{\beta}^*}{2} \|\tilde{F} \tilde{m} - y\|_2^2 - \frac{\tilde{\alpha}^*}{2} \tilde{m}^T \tilde{m} - \frac{1}{2} \log |\tilde{A}^*| \\
 &= \frac{n}{2} \log \beta^* + \frac{qD}{2} \log (q\alpha^*) - \frac{n}{2} \log 2\pi - \frac{\beta^*}{2} \|F m - y\|_2^2 - \frac{\alpha^*}{2} m^T m - \frac{1}{2} \log |\tilde{\Lambda}^*| \\
 &= \frac{n}{2} \log \beta^* + \frac{qD}{2} \log (q\alpha^*) - \frac{n}{2} \log 2\pi - \frac{\beta^*}{2} \|F m - y\|_2^2 - \frac{\alpha^*}{2} m^T m \\
 &\quad - \frac{1}{2} \log |\Lambda^*| - \frac{1}{2} \log \left(q^D (q\alpha^*)^{(q-1)D} \right) \\
 &= \mathcal{L} - \frac{D}{2} \log \alpha^* + \frac{qD}{2} \log (q\alpha^*) - \frac{1}{2} \log \left(q^D (q\alpha^*)^{(q-1)D} \right) \\
 &= \mathcal{L}
 \end{aligned}$$

By the convergence analysis in Section 4.1, initialization of α, β only changes the initial value of t , which does not impact the convergence value of the fixed point iteration. Therefore, we can conclude that duplicating features will not change the value of LogME.

Although the above proof targets at Algorithm 2, it is straightforward to adapt the proof to Algorithm 3. \blacksquare

E. Proof of Corollary 4

Corollary 4: LogME value will remain the same if the feature is padded with arbitrary number of zeros. Formally speaking, if the LogME value for $F \in \mathbb{R}^{n \times D}$ and $y \in \mathbb{R}^n$ is \mathcal{L} , then the LogME value for $\tilde{F} = [F, \mathbf{0}] \in \mathbb{R}^{n \times (D+d)}$ and $y \in \mathbb{R}^n$ is also \mathcal{L} . $d \in \mathbb{N}$ is a natural number and $\mathbf{0} \in \mathbb{R}^{n \times d}$ is a matrix with all zero entries.

Proof The proof follows the same idea as Corollary 3, but the SVD of \tilde{F} is simpler than Corollary 3. If the SVD of F is $F = U\Sigma V^T$, then the SVD of $\tilde{F} = [F, \mathbf{0}]$ is $\tilde{F} = \tilde{U}\tilde{\Sigma}\tilde{V}^T$, where $\tilde{U} = U, \tilde{\Sigma} = [\Sigma, \mathbf{0}], \tilde{V} = \begin{bmatrix} V \\ W \end{bmatrix}$, with $W \in \mathbb{R}^{d \times d}$ an orthogonal matrix that satisfies $W^T W = I_d$. Note that $\tilde{\Sigma} = [\Sigma, \mathbf{0}]$ translates into $\tilde{\sigma}_i^2 = \begin{cases} \sigma_i^2 & 1 \leq i \leq D \\ 0 & D+1 \leq i \leq D+d \end{cases}$.

Iterative invariant: if we apply Algorithm 2 to both \tilde{F} and F , with the same initialization $\tilde{\alpha} = 1, \tilde{\beta} = 1$, then $\tilde{\alpha} = \alpha, \tilde{\beta} = \beta$ holds before Line 5. Suppose $\tilde{\alpha} = \alpha, \tilde{\beta} = \beta$ holds before a while-loop, then we can have:

$$\begin{aligned} \tilde{\gamma} &= \sum_{i=1}^{D+d} \frac{\tilde{\beta} \tilde{\sigma}_i^2}{\tilde{\alpha} + \tilde{\beta} \tilde{\sigma}_i^2} = \sum_{i=1}^D \frac{\beta \sigma_i^2}{\alpha + \beta \sigma_i^2} = \gamma \\ \tilde{\Lambda} &= \text{diag} \left\{ \tilde{\alpha} + \tilde{\beta} \tilde{\sigma}_i^2 \right\}, \tilde{\alpha} + \tilde{\beta} \tilde{\sigma}_i^2 = \begin{cases} \alpha + \beta \sigma_i^2 & 1 \leq i \leq D \\ \alpha & D+1 \leq i \leq D+d \end{cases} \end{aligned}$$

$$\begin{aligned} \tilde{m} &= \tilde{\beta} \tilde{A}^{-1} \tilde{F}^T y = \beta \begin{bmatrix} V & W \end{bmatrix} \begin{bmatrix} \Lambda^{-1} & \\ & \frac{1}{\alpha} I_d \end{bmatrix} \begin{bmatrix} V^T & \\ & W^T \end{bmatrix} \begin{bmatrix} F^T \\ \mathbf{0}_{n \times d}^T \end{bmatrix} y = \begin{bmatrix} m \\ \mathbf{0}_{d \times 1} \end{bmatrix} \\ \tilde{m}^T \tilde{m} &= m^T m, \tilde{F} \tilde{m} = [F, \mathbf{0}_{n \times d}] \begin{bmatrix} m \\ \mathbf{0}_{d \times 1} \end{bmatrix} = Fm \end{aligned}$$

After the while-loop iteration, $\tilde{\alpha}' = \frac{\tilde{\gamma}}{\tilde{m}^T \tilde{m}} = \frac{\gamma}{m^T m} = \alpha', \tilde{\beta}' = \frac{n-\tilde{\gamma}}{\|\tilde{F} \tilde{m} - y\|_2^2} = \frac{n-\gamma}{\|Fm - y\|_2^2} = \beta'$, then the iterative invariant $\tilde{\alpha} = \alpha, \tilde{\beta} = \beta$ still holds. Therefore, we know that when the algorithm converges, $\tilde{\alpha}^* = \alpha^*, \tilde{\beta}^* = \beta^*$. The corresponding maximum evidence is

$$\begin{aligned} \tilde{\mathcal{L}} &= \frac{n}{2} \log \tilde{\beta}^* + \frac{D+d}{2} \log \tilde{\alpha}^* - \frac{n}{2} \log 2\pi - \frac{\tilde{\beta}^*}{2} \|\tilde{F} \tilde{m} - y\|_2^2 - \frac{\tilde{\alpha}^*}{2} \tilde{m}^T \tilde{m} - \frac{1}{2} \log |\tilde{A}^*| \\ &= \frac{n}{2} \log \beta^* + \frac{D+d}{2} \log \alpha^* - \frac{n}{2} \log 2\pi - \frac{\beta^*}{2} \|Fm - y\|_2^2 - \frac{\alpha^*}{2} m^T m - \frac{1}{2} \log |\tilde{\Lambda}^*| \\ &= \frac{n}{2} \log \beta^* + \frac{D+d}{2} \log \alpha^* - \frac{n}{2} \log 2\pi - \frac{\beta^*}{2} \|Fm - y\|_2^2 - \frac{\alpha^*}{2} m^T m \\ &\quad - \frac{1}{2} \log |\Lambda^*| - \frac{1}{2} \log (\alpha^*)^d \\ &= \mathcal{L} + \frac{d}{2} \log \alpha^* - \frac{d}{2} \log \alpha^* \\ &= \mathcal{L} \end{aligned}$$

■

F. Detailed descriptions of the datasets

Aircraft: The dataset contains fine-grained classification of 10,000 aircraft pictures which belong to 100 classes, with 100 images per class.

Birdsnap: The dataset contains 49,829 images of 500 species of North American birds.

Caltech: The dataset contains 9,144 pictures of objects belonging to 101 categories. There are about 40 to 800 images per category. Most categories have about 50 images.

Cars: The dataset contains 16,185 images of 196 classes of cars. The data is split into 8,144 training images and 8,041 testing images.

CIFAR 10: The dataset consists of 60,000 32×32 colorful images in 10 classes, with 6,000 images per class. There are 50,000 training images and 10,000 test images.

CIFAR 100: The dataset is just like the CIFAR 10, except it has 100 classes containing 600 images each.

DTD: The dataset contains a collection of 5,640 textural images in the wild, annotated with a series of human-centric attributes. It has 47 classes and 120 images per class.

Pets: The dataset contains 7,049 images of cat and dog species which belong to 47 classes, with around 200 images per class.

SUN: The dataset contains 39,700 scenery pictures with 397 classes and 100 samples per class.

G. Original Results in Figures

Original results in figures are shown in the Table 10, Table 11, and Table 12.

Table 10: Original results in Figure 4.

task	ResNet-34	ResNet-50	ResNet-101	ResNet-152	WideResNet-50	DenseNet-121	DenseNet-169	DenseNet-201	Inception v1	Inception v3	MobileNet v2	NASNet-A	Mobile	τ_w
Aircraft	Accuracy	79.9	86.6	85.6	85.3	83.2	85.4	84.5	84.6	82.7	88.8	82.8	72.8	-
	Laplace	-2.864	-3.127	-3.080	-3.158	-3.721	-2.235	-1.906	-1.754	-2.382	-2.822	-2.217	-1.481	-0.32
	LEEP	-0.497	-0.412	-0.349	-0.308	-0.337	-0.431	-0.340	-0.462	-0.795	-0.492	-0.515	-0.506	0.13
	NCE	-0.364	-0.297	-0.244	-0.214	-0.248	-0.296	-0.259	-0.322	-0.348	-0.250	-0.411	-0.444	0.39
Birdsnap	LogME	0.930	0.946	0.948	0.950	0.934	0.938	0.943	0.942	0.934	0.953	0.941	0.948	0.59
	Accuracy	59.5	74.7	73.8	74.3	63.1	73.2	71.4	72.6	73.0	77.2	69.3	68.3	-
	LEEP	-1.758	-1.647	-1.553	-1.481	-1.554	-1.729	-1.756	-1.645	-2.483	-1.776	-1.951	-1.835	0.19
	NCE	-1.640	-1.538	-1.479	-1.417	-1.399	-1.566	-1.644	-1.493	-1.807	-1.354	-1.815	-1.778	0.51
Caltech	LogME	0.802	0.829	0.836	0.839	0.825	0.810	0.815	0.822	0.806	0.848	0.808	0.824	0.66
	Accuracy	90.2	91.8	93.1	93.2	91.0	91.9	92.5	93.4	91.7	94.3	89.1	91.5	-
	LEEP	-2.249	-2.195	-2.067	-1.984	-2.179	-2.159	-2.039	-2.122	-2.718	-2.286	-2.373	-2.263	0.30
	NCE	-1.899	-1.820	-1.777	-1.721	-1.828	-1.807	-1.774	-1.808	-1.849	-1.722	-2.009	-1.966	0.69
Cars	LogME	1.362	1.509	1.548	1.567	1.505	1.365	1.417	1.428	1.440	1.605	1.365	1.389	0.66
	Accuracy	86.4	91.7	91.7	92.0	89.7	91.5	91.5	91.0	91.0	92.3	91.0	88.5	-
	LEEP	-1.534	-1.570	-1.370	-1.334	-1.406	-1.562	-1.505	-1.687	-2.149	-1.637	-1.695	-1.588	0.26
	NCE	-1.203	-1.181	-1.142	-1.128	-1.183	-1.111	-1.192	-1.319	-1.201	-1.195	-1.312	-1.334	0.36
CIFAR10	LogME	1.245	1.253	1.255	1.260	1.250	1.249	1.252	1.251	1.246	1.259	1.250	1.254	0.69
	Accuracy	97.1	96.8	97.7	97.9	97.7	97.2	97.4	97.4	96.2	97.5	95.7	96.8	-
	LEEP	-3.418	-3.407	-3.184	-3.020	-3.335	-3.651	-3.345	-3.458	-4.074	-3.976	-3.624	-3.467	0.72
	NCE	-3.398	-3.395	-3.232	-3.084	-3.348	-3.541	-3.427	-3.467	-3.338	-3.625	-3.511	-3.436	0.51
CIFAR100	LogME	0.323	0.388	0.463	0.469	0.398	0.302	0.343	0.369	0.293	0.349	0.291	0.304	0.82
	Accuracy	84.5	84.5	87.0	87.6	86.4	84.8	85.0	86.0	83.2	86.6	80.8	83.9	-
	LEEP	-3.531	-3.520	-3.330	-3.167	-3.391	-3.715	-3.525	-3.643	-4.279	-4.100	-3.733	-3.560	0.66
	NCE	-3.230	-3.241	-3.112	-2.980	-3.158	-3.304	-3.313	-3.323	-3.253	-3.447	-3.336	-3.254	0.53
DTD	LogME	1.036	1.099	1.130	1.133	1.102	1.029	1.051	1.061	1.037	1.070	1.039	1.051	0.77
	Accuracy	70.0	75.2	76.2	75.4	70.1	74.9	74.8	74.5	73.6	77.2	72.9	72.8	-
	LEEP	-3.670	-3.663	-3.718	-3.653	-3.764	-3.847	-3.646	-3.757	-4.124	-4.096	-3.805	-3.691	-0.06
	NCE	-3.104	-3.119	-3.199	-3.138	-3.259	-3.198	-3.218	-3.203	-3.082	-3.261	-3.176	-3.149	-0.35
Pets	LogME	0.704	0.761	0.757	0.766	0.731	0.710	0.730	0.730	0.727	0.746	0.712	0.724	0.50
	Accuracy	92.3	92.5	94.0	94.5	92.8	92.9	93.1	92.8	91.9	93.5	90.5	89.4	-
	LEEP	-1.174	-1.031	-0.915	-0.892	-0.945	-1.100	-1.111	-1.108	-1.520	-1.129	-1.228	-1.150	0.66
	NCE	-1.094	-0.956	-0.885	-0.862	-0.900	-0.987	-1.072	-1.026	-1.076	-0.893	-1.156	-1.146	0.83
SUN	LogME	0.835	1.029	1.061	1.084	1.016	0.839	0.874	0.908	0.913	1.191	0.821	0.833	0.61
	Accuracy	63.1	64.7	64.8	66.0	67.4	62.3	63.0	64.7	62.0	65.7	60.5	60.7	-
	LEEP	-2.727	-2.611	-2.531	-2.513	-2.569	-2.713	-2.570	-2.618	-3.153	-2.943	-2.764	-2.687	0.54
	NCE	-2.573	-2.469	-2.455	-2.444	-2.457	-2.500	-2.480	-2.465	-2.534	-2.529	-2.590	-2.586	0.68
	LogME	1.704	1.744	1.749	1.755	1.750	1.704	1.716	1.718	1.715	1.753	1.713	1.721	0.71

Table 11: Original results in Figure 5.

task	ResNet-34	ResNet-50	ResNet-101	ResNet-152	WideResNet-50	DenseNet-121	DenseNet-169	DenseNet-201	Inception v1	Inception v3	MobileNet v2	NASNet-A	Mobile	τ_w
dSprites	MSE	0.037	0.031	0.028	0.028	0.034	0.039	0.035	0.036	0.045	0.044	0.037	0.035	-
	LogME	1.05	1.53	1.64	1.63	1.31	1.35	1.25	1.34	1.18	1.22	1.18	1.39	0.79

Table 12: Original results in Figure 9. (Popularity is measured by download count in millions.)

	task	RoBERTa	RoBERTa-D	uncased BERT-D	cased BERT-D	ALBERT-v1	ALBERT-v2	ELECTRA-base	ELECTRA-small	τ_w
MNLI	Accuracy	87.6	84.0	82.2	81.5	81.6	84.6	79.7	85.8	-
	LogME	-0.568	-0.599	-0.603	-0.612	-0.614	-0.594	-0.666	-0.621	0.66
	Popularity	3.78	0.61	6.01	1.09	0.11	1.25	0.13	0.23	0.28
QQP	Accuracy	91.9	89.4	88.5	87.8	-	-	-	-	-
	LogME	-0.465	-0.492	-0.488	-0.521	-	-	-	-	0.73
	Popularity	3.78	0.61	6.01	1.09	-	-	-	-	0.00
QNLI	Accuracy	92.8	90.8	89.2	88.2	-	-	-	-	-
	LogME	-0.565	-0.603	-0.613	-0.618	-	-	-	-	1.00
	Popularity	3.78	0.61	6.01	1.09	-	-	-	-	0.00
SST-2	Accuracy	94.8	92.5	91.3	90.4	90.3	92.9	-	-	-
	LogME	-0.312	-0.330	-0.331	-0.353	-0.525	-0.447	-	-	0.68
	Popularity	3.78	0.61	6.01	1.09	0.11	1.25	-	-	0.38
CoLA	Accuracy	63.6	59.3	51.3	47.2	-	-	-	-	-
	LogME	-0.499	-0.536	-0.568	-0.572	-	-	-	-	1.00
	Popularity	3.78	0.61	6.01	1.09	-	-	-	-	0.00
MRPC	Accuracy	90.2	86.6	87.5	85.6	-	-	-	-	-
	LogME	-0.573	-0.586	-0.605	-0.604	-	-	-	-	0.53
	Popularity	3.78	0.61	6.01	1.09	-	-	-	-	0.33
RTE	Accuracy	78.7	67.9	59.9	60.6	-	-	-	-	-
	LogME	-0.709	-0.723	-0.725	-0.725	-	-	-	-	1.00
	Popularity	3.78	0.61	6.01	1.09	-	-	-	-	-0.29

H. Complete results in prompt learning

Table 13: Complete results in prompt learning with manually selected anchor words.

accuracy \ anchor N	negative	bad	ill	evil	poor
anchor P					
positive	49.8	52.8	49.1	49.1	60.9
good	51.0	50.9	49.0	52.4	50.9
fine	51.7	51.0	49.1	54.5	50.9
great	55.4	53.1	49.1	61.4	51.0
nice	51.6	50.6	49.1	51.0	50.8

I. Full Figure in Convergence Analysis

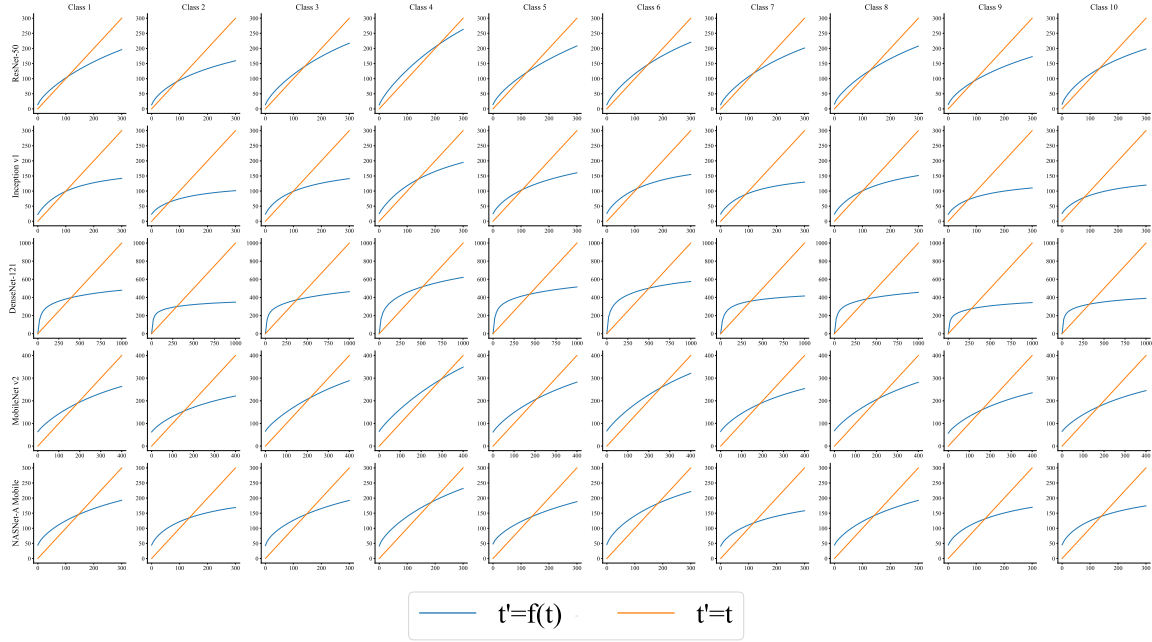


Figure 13: Fixed points of $f(t)$ in Equation 3 for all 10 classes in CIFAR10 with 5 pre-trained models. We plot $t' = f(t)$ (in blue) and $t' = t$ (in orange), whose intersections are fixed points. The existence of fixed points guarantees the convergence of the evidence maximization procedure in LogME.

References

S. Ben-David and R. Schuller. Exploiting task relatedness for multiple task learning. In *COLT*, pages 567–580, Berlin, Heidelberg, 2003.

T. Berg, J. Liu, S. Woo Lee, M. L. Alexander, D. W. Jacobs, and P. N. Belhumeur. Birdsnap: Large-scale fine-grained visual categorization of birds. In *CVPR*, pages 2011–2018, Columbus, Ohio, 2014.

C. M. Bishop. *Neural networks for pattern recognition*. Oxford University Press, 1995.

C. M. Bishop. *Pattern recognition and machine learning*. Springer, New York, 2006.

R. Bommasani, D. A. Hudson, E. Adeli, R. Altman, S. Arora, S. von Arx, M. S. Bernstein, J. Bohg, A. Bosselut, E. Brunskill, E. Brynjolfsson, S. Buch, D. Card, R. Castellon, N. Chatterji, A. Chen, K. Creel, J. Q. Davis, D. Demszky, C. Donahue, M. Doumbouya, E. Durmus, S. Ermon, J. Etchemendy, K. Ethayarajh, L. Fei-Fei, C. Finn, T. Gale, L. Gillespie, K. Goel, N. Goodman, S. Grossman, N. Guha, T. Hashimoto, P. Henderson, J. Hewitt, D. E. Ho, J. Hong, K. Hsu, J. Huang, T. Icard, S. Jain, D. Jurafsky, P. Kalluri, S. Karamcheti, G. Keeling, F. Khani, O. Khattab, P. W. Kohd, M. Krass, R. Krishna, R. Kuditipudi, A. Kumar, F. Ladhak, M. Lee, T. Lee, J. Leskovec, I. Levent, X. L. Li, X. Li, T. Ma, A. Malik, C. D. Manning, S. Mirchandani, E. Mitchell, Z. Munyikwa, S. Nair, A. Narayan, D. Narayanan, B. Newman, A. Nie, J. C. Niebles, H. Nilforoshan, J. Nyarko, G. Ogut, L. Orr, I. Papadimitriou, J. S. Park, C. Piech, E. Portelance, C. Potts, A. Raghunathan, R. Reich, H. Ren, F. Rong, Y. Roohani, C. Ruiz, J. Ryan, C. Ré, D. Sadigh, S. Sagawa, K. Santhanam, A. Shih, K. Srinivasan, A. Tamkin, R. Taori, A. W. Thomas, F. Tramèr, R. E. Wang, W. Wang, B. Wu, J. Wu, Y. Wu, S. M. Xie, M. Yasunaga, J. You, M. Zaharia, M. Zhang, T. Zhang, X. Zhang, Y. Zhang, L. Zheng, K. Zhou, and P. Liang. On the Opportunities and Risks of Foundation Models. *arXiv:2108.07258 [cs]*, 2021.

T. Brown, B. Mann, N. Ryder, M. Subbiah, J. D. Kaplan, P. Dhariwal, A. Neelakantan, P. Shyam, G. Sastry, A. Askell, S. Agarwal, A. Herbert-Voss, G. Krueger, T. Henighan, R. Child, A. Ramesh, D. Ziegler, J. Wu, C. Winter, C. Hesse, M. Chen, E. Sigler, M. Litwin, S. Gray, B. Chess, J. Clark, C. Berner, S. McCandlish, A. Radford, I. Sutskever, and D. Amodei. Language Models are Few-Shot Learners. In *NeurIPS*, pages 1877–1901, Online, 2020.

Z. Cao, K. You, Z. Zhang, J. Wang, and M. Long. From Big to Small: Adaptive Learning to Partial-Set Domains. *TPAMI*, 2022. early access.

L.-C. Chen, G. Papandreou, F. Schroff, and H. Adam. Rethinking Atrous Convolution for Semantic Image Segmentation. *arXiv:1706.05587 [cs]*, 2017.

T. Chen, S. Kornblith, M. Norouzi, and G. Hinton. A Simple Framework for Contrastive Learning of Visual Representations. In *ICML*, pages 1597–1607, Online, 2020a.

X. Chen, S. Wang, B. Fu, M. Long, and J. Wang. Catastrophic Forgetting Meets Negative Transfer: Batch Spectral Shrinkage for Safe Transfer Learning. In *NeurIPS*, page 1906–1916, Vancouver, Canada, 2019.

X. Chen, H. Fan, R. Girshick, and K. He. Improved Baselines with Momentum Contrastive Learning. *arXiv:2003.04297 [cs]*, 2020b.

M. Cimpoi, S. Maji, I. Kokkinos, S. Mohamed, and A. Vedaldi. Describing textures in the wild. In *CVPR*, page 3606–3613, Columbus, Ohio, 2014.

K. Clark, M.-T. Luong, Q. V. Le, and C. D. Manning. ELECTRA: Pre-training Text Encoders as Discriminators Rather Than Generators. In *ICLR*, Online, 2020.

T. M. Cover. *Elements of information theory*. John Wiley & Sons, 1999.

J. Daunizeau. Semi-analytical approximations to statistical moments of sigmoid and softmax mappings of normal variables. *arXiv preprint arXiv:1703.00091*, 2017.

A. P. Dempster, N. M. Laird, and D. B. Rubin. Maximum likelihood from incomplete data via the EM algorithm. *Journal of the Royal Statistical Society: Series B (Methodological)*, 39(1):1–22, 1977.

J. Deng, W. Dong, R. Socher, L.-J. Li, K. Li, and L. Fei-Fei. Imagenet: A large-scale hierarchical image database. In *CVPR*, page 248–255, Miami Beach, Florida, 2009.

J. Devlin, M.-W. Chang, K. Lee, and K. Toutanova. BERT: Pre-training of Deep Bidirectional Transformers for Language Understanding. In *NAACL*, page 4171–4186, Minneapolis, Minnesota, 2019.

J. Donahue, Y. Jia, O. Vinyals, J. Hoffman, N. Zhang, E. Tzeng, and T. Darrell. Decaf: A deep convolutional activation feature for generic visual recognition. In *ICML*, page 647–655, Beijing, China, 2014.

A. Dosovitskiy, L. Beyer, A. Kolesnikov, D. Weissenborn, X. Zhai, T. Unterthiner, M. Dehghani, M. Minderer, G. Heigold, S. Gelly, J. Uszkoreit, and N. Houlsby. An Image is Worth 16x16 Words: Transformers for Image Recognition at Scale. In *ICLR*, Online, 2021.

D. Erhan, A. Courville, Y. Bengio, and P. Vincent. Why does unsupervised pre-training help deep learning? In *AISTATS*, page 201–208, Sardinia, Italy, 2010.

R. Fagin, R. Kumar, and D. Sivakumar. Comparing top k lists. In *SODA*, page 28–36, Baltimore, Maryland, 2003.

L. Fei-Fei, R. Fergus, and P. Perona. Learning generative visual models from few training examples: An incremental bayesian approach tested on 101 object categories. In *CVPR Workshops*, page 178–178, Washington D.C., 2004.

Y. Ganin and V. Lempitsky. Unsupervised Domain Adaptation by Backpropagation. In *ICML*, pages 1180–1189, Lille, France, 2015.

R. Girshick, J. Donahue, T. Darrell, and J. Malik. Rich feature hierarchies for accurate object detection and semantic segmentation. In *CVPR*, page 580–587, Columbus, Ohio, 2014.

S. F. Gull. Developments in maximum entropy data analysis. In *Maximum entropy and Bayesian methods*. 1989.

M. Gutmann and A. Hyvärinen. Noise-contrastive estimation: A new estimation principle for unnormalized statistical models. In *AISTATS*, pages 297–304, Sardinia, Italy, 2010.

X. Han, Z. Zhang, N. Ding, Y. Gu, X. Liu, Y. Huo, J. Qiu, L. Zhang, W. Han, M. Huang, Q. Jin, Y. Lan, Y. Liu, Z. Liu, Z. Lu, X. Qiu, R. Song, J. Tang, J.-R. Wen, J. Yuan, W. X. Zhao, and J. Zhu. Pre-Trained Models: Past, Present and Future. *arXiv:2106.07139 [cs]*, 2021.

G. H. Hardy, J. E. Littlewood, G. Pólya, and G. Pólya. *Inequalities*, volume 30. Springer Science & Business Media, 1952.

K. He, X. Zhang, S. Ren, and J. Sun. Delving deep into rectifiers: Surpassing human-level performance on imagenet classification. In *ICCV*, page 1026–1034, Santiago, Chile, 2015.

K. He, X. Zhang, S. Ren, and J. Sun. Deep residual learning for image recognition. In *CVPR*, page 770–778, Las Vegas, Nevada, 2016.

K. He, G. Gkioxari, P. Dollár, and R. Girshick. Mask R-CNN. In *ICCV*, pages 2980–2988, Venice, Italy, 2017.

K. He, H. Fan, Y. Wu, S. Xie, and R. Girshick. Momentum contrast for unsupervised visual representation learning. In *CVPR*, pages 9729–9738, Online, 2020.

G. Hinton, O. Vinyals, and J. Dean. Distilling the knowledge in a neural network. *arXiv:1503.02531*, 2015.

W. Hu, B. Liu, J. Gomes, M. Zitnik, P. Liang, V. Pande, and J. Leskovec. Strategies for Pre-training Graph Neural Networks. In *ICLR*, Online, 2020.

G. Huang, Z. Liu, K. Q. Weinberger, and L. van der Maaten. Densely connected convolutional networks. In *CVPR*, pages 4700–4708, Hawaii, USA, 2017.

A. Immer, M. Bauer, V. Fortuin, G. Rätsch, and K. M. Emtiyaz. Scalable marginal likelihood estimation for model selection in deep learning. In *ICML*, page 4563–4573, Online, 2021.

L. Jing and Y. Tian. Self-supervised visual feature learning with deep neural networks: A survey. *TPAMI*, 43(11):4037–4058, 2020.

N. P. Jouppi, C. Young, N. Patil, D. Patterson, G. Agrawal, R. Bajwa, S. Bates, S. Bhatia, N. Boden, and A. Borchers. In-datacenter performance analysis of a tensor processing unit. In *ISCA*, pages 1–12, Toronto, Canada, 2017.

M. G. Kendall. A new measure of rank correlation. *Biometrika*, 30(1):81–93, 1938.

K. H. Knuth, M. Habeck, N. K. Malakar, A. M. Mubeen, and B. Placek. Bayesian Evidence and Model Selection. *Digital Signal Processing*, 47:50–67, 2015.

D. Koller and N. Friedman. *Probabilistic graphical models: principles and techniques*. MIT press, Cambridge, Massachusetts, 2009.

S. Kornblith, J. Shlens, and Q. V. Le. Do better imagenet models transfer better? In *CVPR*, page 2661–2671, Los Angeles, California, 2019.

Z. Kou, K. You, M. Long, and J. Wang. Stochastic Normalization. In *NeurIPS*, pages 16304–16314, Online, 2020.

J. Krause, J. Deng, M. Stark, and L. Fei-Fei. Collecting a large-scale dataset of fine-grained cars. Technical report, 2013.

A. Krizhevsky and G. Hinton. Learning multiple layers of features from tiny images. Technical report, 2009.

Z. Lan, M. Chen, S. Goodman, K. Gimpel, P. Sharma, and R. Soricut. ALBERT: A Lite BERT for Self-supervised Learning of Language Representations. In *ICLR*, Online, 2020.

C. Li, Y. Mao, R. Zhang, and J. Huai. On hyper-parameter estimation in empirical Bayes: a revisit of the MacKay algorithm. In *UAI*, page 477–486, Arlington, Virginia, 2016.

H. Li, P. Chaudhari, H. Yang, M. Lam, A. Ravichandran, R. Bhotika, and S. Soatto. Rethinking the Hyperparameters for Fine-tuning. In *ICLR*, Online, 2020.

X. Li, Y. Grandvalet, and F. Davoine. Explicit Inductive Bias for Transfer Learning with Convolutional Networks. In *ICML*, pages 2825–2834, Stockholm, Sweden, 2018.

T.-Y. Lin, M. Maire, S. Belongie, J. Hays, P. Perona, D. Ramanan, P. Dollár, and C. L. Zitnick. Microsoft coco: Common objects in context. In *ECCV*, page 740–755, Zurich, Switzerland, 2014.

P. Liu, W. Yuan, J. Fu, Z. Jiang, H. Hayashi, and G. Neubig. Pre-train, Prompt, and Predict: A Systematic Survey of Prompting Methods in Natural Language Processing. *arXiv:2107.13586 [cs]*, 2021a.

Y. Liu, M. Ott, N. Goyal, J. Du, M. Joshi, D. Chen, O. Levy, M. Lewis, L. Zettlemoyer, and V. Stoyanov. Roberta: A robustly optimized bert pretraining approach. *arXiv preprint arXiv:1907.11692*, 2019.

Z. Liu, Y. Lin, Y. Cao, H. Hu, Y. Wei, Z. Zhang, S. Lin, and B. Guo. Swin Transformer: Hierarchical Vision Transformer Using Shifted Windows. In *ICCV*, pages 10012–10022, Montreal, Canada, 2021b.

M. Long, Y. Cao, J. Wang, and M. Jordan. Learning Transferable Features with Deep Adaptation Networks. In *ICML*, pages 97–105, Lille, France, 2015.

D. J. MacKay. Bayesian interpolation. *Neural computation*, 4(3):415–447, 1992.

D. Mahajan, R. Girshick, V. Ramanathan, K. He, M. Paluri, Y. Li, A. Bharambe, and L. van der Maaten. Exploring the limits of weakly supervised pretraining. In *ECCV*, page 181–196, Munich, Germany, 2018.

S. Maji, E. Rahtu, J. Kannala, M. Blaschko, and A. Vedaldi. Fine-Grained Visual Classification of Aircraft. *arXiv:1306.5151 [cs]*, 2013.

L. Matthey, I. Higgins, D. Hassabis, and A. Lerchner. dsprites: Disentanglement testing sprites dataset. Technical report, 2017.

S. Merity, C. Xiong, J. Bradbury, and R. Socher. Pointer Sentinel Mixture Models. In *ICLR*, Toulon, France, 2017.

K. P. Murphy. *Machine learning: a probabilistic perspective*. MIT press, Cambridge, Massachusetts, 2012.

B. Neyshabur, H. Sedghi, and C. Zhang. What is being transferred in transfer learning? In *NeurIPS*, pages 512–523, Online, 2020.

C. Nguyen, T. Hassner, M. Seeger, and C. Archambeau. LEEP: A New Measure to Evaluate Transferability of Learned Representations. In *ICML*, pages 7294–7305, Online, 2020.

O. M. Parkhi, A. Vedaldi, A. Zisserman, and C. V. Jawahar. Cats and dogs. In *CVPR*, pages 3498–3505, Providence, Rhode Island, 2012.

X. Qiu, T. Sun, Y. Xu, Y. Shao, N. Dai, and X. Huang. Pre-trained models for natural language processing: A survey. *Science China Technological Sciences*, 63(10):1872–1897, 2020.

J. Quionero-Candela, M. Sugiyama, A. Schwaighofer, and N. D. Lawrence. *Dataset shift in machine learning*. MIT Press, Cambridge, Massachusetts, 2009.

P. Rajpurkar, J. Zhang, K. Lopyrev, and P. Liang. SQuAD: 100,000+ Questions for Machine Comprehension of Text. In *EMNLP*, page 2383–2392, Austin, Texas, 2016.

C. E. Rasmussen. Gaussian processes in machine learning. In *Summer school on machine learning*, pages 63–71, Berlin, Heidelberg, 2003.

O. Russakovsky, J. Deng, H. Su, J. Krause, S. Satheesh, S. Ma, Z. Huang, A. Karpathy, A. Khosla, and M. Bernstein. Imagenet large scale visual recognition challenge. *IJCV*, 115(3):211–252, 2015.

M. Sandler, A. Howard, M. Zhu, A. Zhmoginov, and L.-C. Chen. MobileNetV2: Inverted Residuals and Linear Bottlenecks. In *CVPR*, pages 4510–4520, Salt Lake City, Utah, 2018.

E. T. K. Sang and F. De Meulder. Introduction to the CoNLL-2003 Shared Task: Language-Independent Named Entity Recognition. In *NAACL*, page 142–147, Edmonton, Canada, 2003.

V. Sanh, L. Debut, J. Chaumond, and T. Wolf. DistilBERT, a distilled version of BERT: smaller, faster, cheaper and lighter. *arXiv:1910.01108*, 2019.

Y. Shu, Z. Kou, Z. Cao, J. Wang, and M. Long. Zoo-Tuning: Adaptive Transfer from A Zoo of Models. In *ICML*, pages 9626–9637, Online, 2021.

S. P. Singh and M. Jaggi. Model fusion via optimal transport. In *NeurIPS*, pages 22045–22055, Online, 2020.

R. Socher, A. Perelygin, J. Wu, J. Chuang, C. D. Manning, A. Y. Ng, and C. Potts. Recursive deep models for semantic compositionality over a sentiment treebank. In *EMNLP*, page 1631–1642, Seattle, USA, 2013.

C. Sun, A. Shrivastava, S. Singh, and A. Gupta. Revisiting unreasonable effectiveness of data in deep learning era. In *ICCV*, page 843–852, Venice, Italy, 2017.

C. Szegedy, W. Liu, Y. Jia, P. Sermanet, S. Reed, D. Anguelov, D. Erhan, V. Vanhoucke, and A. Rabinovich. Going deeper with convolutions. pages 1–9, Boston, Massachusetts, 2015.

C. Szegedy, V. Vanhoucke, S. Ioffe, J. Shlens, and Z. Wojna. Rethinking the Inception Architecture for Computer Vision. In *CVPR*, pages 2818–2826, Las Vegas, Nevada, 2016.

M. Tan, B. Chen, R. Pang, V. Vasudevan, M. Sandler, A. Howard, and Q. V. Le. Mnasnet: Platform-aware neural architecture search for mobile. In *CVPR*, page 2820–2828, Los Angeles, California, 2019.

S. Thrun and L. Pratt. Learning to Learn: Introduction and Overview. In *Learning to Learn*, pages 3–17, Boston, Massachusetts, 1998.

Y. Tian, C. Sun, B. Poole, D. Krishnan, C. Schmid, and P. Isola. What Makes for Good Views for Contrastive Learning? In *NeurIPS*, pages 6827–6839, Online, 2020.

I. O. Tolstikhin, N. Houlsby, A. Kolesnikov, L. Beyer, X. Zhai, T. Unterthiner, J. Yung, A. Steiner, D. Keysers, and J. Uszkoreit. Mlp-mixer: An all-mlp architecture for vision. In *NeurIPS*, pages 24261–24272, Online, 2021.

A. T. Tran, C. V. Nguyen, and T. Hassner. Transferability and hardness of supervised classification tasks. In *ICCV*, page 1395–1405, Seoul, Korea, 2019.

S. Vigna. A Weighted Correlation Index for Rankings with Ties. In *WWW*, pages 1166–1176, Florence, Italy, 2015.

A. Wang, A. Singh, J. Michael, F. Hill, O. Levy, and S. R. Bowman. GLUE: A Multi-Task Benchmark and Analysis Platform for Natural Language Understanding. In *EMNLP*, page 353–355, Brussels, Belgium, 2018.

A. Wang, Y. Pruksachatkun, N. Nangia, A. Singh, J. Michael, F. Hill, O. Levy, and S. R. Bowman. SuperGLUE: A Stickier Benchmark for General-Purpose Language Understanding Systems. In *NeurIPS*, Vancouver, Canada, 2019.

T. Wolf, J. Chaumond, L. Debut, V. Sanh, C. Delangue, A. Moi, P. Cistac, M. Funtowicz, J. Davison, and S. Shleifer. Transformers: State-of-the-art natural language processing. In *EMNLP*, pages 38–45, Online, 2020.

J. Xiao, J. Hays, K. A. Ehinger, A. Oliva, and A. Torralba. Sun database: Large-scale scene recognition from abbey to zoo. In *CVPR*, pages 3485–3492, San Francisco, California, 2010.

Z. Yang, Z. Dai, Y. Yang, J. Carbonell, R. R. Salakhutdinov, and Q. V. Le. Xlnet: Generalized autoregressive pretraining for language understanding. In *NeurIPS*, Vancouver, Canada, 2019.

J. Yosinski, J. Clune, Y. Bengio, and H. Lipson. How transferable are features in deep neural networks? In *NeurIPS*, page 3320–3328, Montreal, Canada, 2014.

K. You, Z. Kou, M. Long, and J. Wang. Co-Tuning for Transfer Learning. In *NeurIPS*, pages 17236–17246, Online, 2020.

K. You, Y. Liu, J. Wang, and M. Long. LogME: Practical Assessment of Pre-trained Models for Transfer Learning. In *ICML*, pages 12133–12143, Online, 2021.

S. Zagoruyko and N. Komodakis. Wide Residual Networks. In *BMVC*, York, UK, 2016.

A. R. Zamir, A. Sax, W. Shen, L. J. Guibas, J. Malik, and S. Savarese. Taskonomy: Disentangling Task Transfer Learning. In *CVPR*, pages 3712–3722, Salt Lake City, Utah, 2018.

X. Zhai, J. Puigcerver, A. Kolesnikov, P. Ruyssen, C. Riquelme, M. Lucic, J. Djolonga, A. S. Pinto, M. Neumann, A. Dosovitskiy, L. Beyer, O. Bachem, M. Tschannen, M. Michalski, O. Bousquet, S. Gelly, and N. Houlsby. A Large-scale Study of Representation Learning with the Visual Task Adaptation Benchmark. *arXiv:1910.04867 [cs, stat]*, 2020.